Developmental Biology 357 (2011) 463–477

Contents lists available at ScienceDirect

Developmental Biology

journal homepage: www.elsevier.com/developmentalbiology

Genomes and Developmental Control

miR-196 regulates axial patterning and pectoral appendage initiation

Xinjun He [a], Yi-Lin Yan [a], Johann K. Eberhart [a,1], Amaury Herpin [b], Toni U. Wagner [b], Manfred Schartl [b], John H. Postlethwait [a,b,*]

[a] Institute of Neuroscience, University of Oregon, Eugene OR 97403 USA
[b] Department of Physiological Chemistry I, Biocenter, University of Wuerzburg, Am Hubland, 97074 Wuerzburg, Germany

ARTICLE INFO

Article history:
Received for publication 30 July 2010
Revised 5 July 2011
Accepted 8 July 2011
Available online 20 July 2011

Keywords:
microRNA (miRNA)
Mir196 (miR-196)
Axial skeletal patterning
Pectoral fin
Pharyngeal arch
Retinoic acid

ABSTRACT

Vertebrate *Hox* clusters contain protein-coding genes that regulate body axis development and microRNA (miRNA) genes whose functions are not yet well understood. We overexpressed the *Hox* cluster microRNA miR-196 in zebrafish embryos and found four specific, viable phenotypes: failure of pectoral fin bud initiation, deletion of the 6th pharyngeal arch, homeotic aberration and loss of rostral vertebrae, and reduced number of ribs and somites. Reciprocally, miR-196 knockdown evoked an extra pharyngeal arch, extra ribs, and extra somites, confirming endogenous roles of miR-196. miR-196 injection altered expression of *hox* genes and the signaling of retinoic acid through the retinoic acid receptor gene *rarab*. Knocking down *rarab* mimicked the pectoral fin phenotype of miR-196 overexpression, and reporter constructs tested in tissue culture and in embryos showed that the *rarab* 3′UTR is a miR-196 target for pectoral fin bud initiation. These results show that a *Hox cluster* microRNA modulates development of axial patterning similar to nearby protein-coding *Hox* genes, and acts on appendicular patterning at least in part by modulating retinoic acid signaling.

Introduction

Hox cluster genes control animal body patterning in radiata and in bilateria, including both protostomes and deuterostomes (Finnerty et al., 2004; Postlethwait and Schneiderman, 1969; Wellik, 2009). In vertebrate deuterostomes, *Hox cluster* genes control the anterior–posterior body axis, including the identity of vertebrae and pharyngeal arches and the axes of body appendages (Krumlauf, 1994), and they are important for the development of mesodermal organ systems (Di-Poi et al., 2010). *Hox* clusters evolved by tandem gene duplication followed by whole genome duplication events in vertebrates that provided tetrapods with four *Hox* clusters and most teleost fish with seven or eight (Amores et al., 1998, 2004; Chambers et al., 2009; Gehring et al., 2009; Graham et al., 1989; Woltering and Durston, 2006).

Hox genes are expressed in a collinear fashion along the anterior–posterior body axis during early development, with genes located 3′ in the cluster controlling anterior development and those located 5′ regulating more posterior organ development (Duboule and Morata, 1994; Graham et al., 1989); as a result, *Hox* gene mutations can delete vertebrae or transform vertebral identity and remove or reduce limb skeletal elements (Chen and Capecchi, 1997; Davis et al., 1995). *Hox* genes act by controlling downstream transcription factors that regulate signaling events controlling body segmentation and organ initiation. Some *Hox* genes are themselves directly regulated by the extracellular signaler retinoic acid (RA), which controls axis and pectoral appendage development (Grandel et al., 2002; Hoffman et al., 2002; Nolte et al., 2003).

Bilaterian *Hox* clusters contain protein-coding genes and genes encoding microRNAs (miRNAs), small non-coding RNAs that generally bind to 3′ untranslated regions (UTRs) of messenger RNAs and regulate their stability or translation (Fjose and Zhao, 2010; Vella et al., 2004). The human genome has three *Hox cluster* miRNA genes, *MIR10*, *MIR196*, and *MIR615*. The *MIR10* gene is broadly distributed among bilaterians; *MIR196* is conserved among vertebrates; and *MIR615* is restricted to mammalian genomes (see miRBase collection at http://www.miRBase.org (Griffiths-Jones et al., 2008; Yekta et al., 2008)). In zebrafish, the *hoxdb* cluster lost all of its protein-coding genes (Amores et al., 1998), but surprisingly, retained *mir10* (Woltering and Durston, 2006). The similarity of *Hox* cluster miRNA expression patterns to those of nearby *hox* genes suggested that *Hox* cluster miRNAs and *Hox* cluster genes share regulatory mechanisms (Wienholds et al., 2005). Furthermore, the discovery that the 3′ UTRs of several *Hox* cluster genes contain predicted binding sites for either miR-196 or miR-10 suggested that some *Hox* genes might be regulated by *Mir10* and/or *Mir196* (He et al., 2009; Hornstein et al.,

* Corresponding author at: Institute of Neuroscience, University of Oregon, Eugene OR 97403 USA. Fax: +1 541 346 4538.
E-mail addresses: xhe@uoneuro.uoregon.edu (X. He), yan@uoneuro.uoregon.edu (Y.-L. Yan), eberhart@mail.utexas.edu (J.K. Eberhart), amaury.herpin@biozentrum.uni-wuerzburg.de (A. Herpin), toni.wagner@biozentrum.uni-wuerzburg.de (T.U. Wagner), phch1@biozentrum.uni-wuerzburg.de (M. Schartl), jpostle@uoneuro.uoregon.edu (J.H. Postlethwait).
[1] Present address: Section of Molecular Cell and Developmental Biology, University of Texas at Austin, TX 78712, USA.

0012-1606/$ – see front matter © 2011 Elsevier Inc. All rights reserved.
doi:10.1016/j.ydbio.2011.07.014

2005; Kawasaki and Taira, 2004; Woltering and Durston, 2008; Yekta et al., 2004; Yekta et al., 2008). For example, *mir10* is involved in the regulation of metastasis by controlling *Hoxd10* in cell culture and *hoxb1a* and *hoxb3a in vivo* (Lund, 2009; Ma et al., 2007; Woltering and Durston, 2008). miR-196 binds to *Hoxb8* mRNA, thereby accelerating its cleavage, and this interaction has been hypothesized to be important for the outgrowth of hindlimb buds (Hornstein et al., 2005; Kawasaki and Taira, 2004; Yekta et al., 2004). In the CNS, miR-196 restricts motor neuron differentiation by regulating *Hoxb8* (Asli and Kessel, 2010). miR-196 is also involved in cancer progression by interaction with other *Hox8* paralogs (Li et al., 2010) (Chen et al., 2011). miRNA-196 can also repress *BACH1* expression in human liver cells (Hou et al., 2010) and is important for tail regeneration in the axolotl (Sehm et al., 2009). Knockdown of miR-196 in chick embryos leads to a homeotic transformation of a cervical vertebra to thoracic identity (McGlinn et al., 2009). Because no phenotype has yet been described for the overexpression of *mir196* in embryos and no phenotype has been described in other tissues where it is expressed, we do not yet fully understand its roles in development or the mechanisms by which it acts.

Here we show that precise levels of *mir196* are required to initiate development of the pectoral appendage, to develop the correct number of pharyngeal arches, and to specify the number and identity of rostral vertebrae and ribs. We show that miR-196 can alter *hox* gene expression patterns and that miR-196 acts on pectoral appendage development by altering retinoic acid signaling via fine-tuning the expression of the retinoic acid receptor Rarab.

Results

mir196 genomics

The human genome has three copies of *MIR196* located between paralogy groups 9 and 10 (Yekta et al., 2008), but due to the teleost genome duplication (Amores et al., 1998; Postlethwait et al., 1998; Taylor et al., 2003), zebrafish has five *mir196* genes (Supplementary Fig. S1A). The teleost whole genome duplication would have initially produced six *mir196* genes, but one of the two *hoxbb mir196* duplicates was lost and duplicates of only the *hoxa* and *hoxc* cluster genes were maintained. The five zebrafish *mir196* paralogs encode four different mature miR-196 sequences with a central nucleotide trio containing (C/G/T) A (A/T). The duplicate *hoxa* and *hoxc* clusters have *mir196* paralogs that differ by one nucleotide [(C/T) AT and (C/G) AT], respectively (Fig. 1A). Because miRNAs often bind their targets with some mismatch (He and Hannon, 2004; Yekta et al., 2004), all four miR-196 sequences probably regulate the same targets.

mir196 expression patterns

mir196 genes and nearby *hox* genes share spatial expression patterns in the central nervous system (CNS) and pectoral fin bud (Wienholds et al., 2005; Woltering and Durston, 2006; Yekta et al., 2008) (compare Fig. 1C–J and Supplementary Fig. S1B–M). This result suggests that *hox* cluster miRNAs may share regulatory mechanisms with neighboring *hox* genes. To investigate temporal aspects of *mir196* expression, we used gene-specific primers for *mir196* primary transcripts and RT-PCR to discover that *mir196a1*(*hoxca*) transcript had begun to accumulate at 24 h post-fertilization (hpf), but *mir196a2* (*hoxaa*) transcript, which encodes the same mature miRNA sequence as *mir196a1*(*hoxca*), was maternally expressed (Fig. 1B). Transcripts from *mir196b*(*hoxba*) and *mir196c*(*hoxcb*) genes first appeared at bud stage, and transcript from *mir196d*(*hoxab*) first accumulated at 5 hpf (Fig. 1B) when gastrulation initiates. This gene-specific timing suggests that different *mir196* genes experience different regulations and may play different roles in development. In addition, whole mount *in situ* hybridization experiments showed that *mir196* genes are expressed in a pattern similar to but different from each other at 24 hpf (Fig. 1C–J).

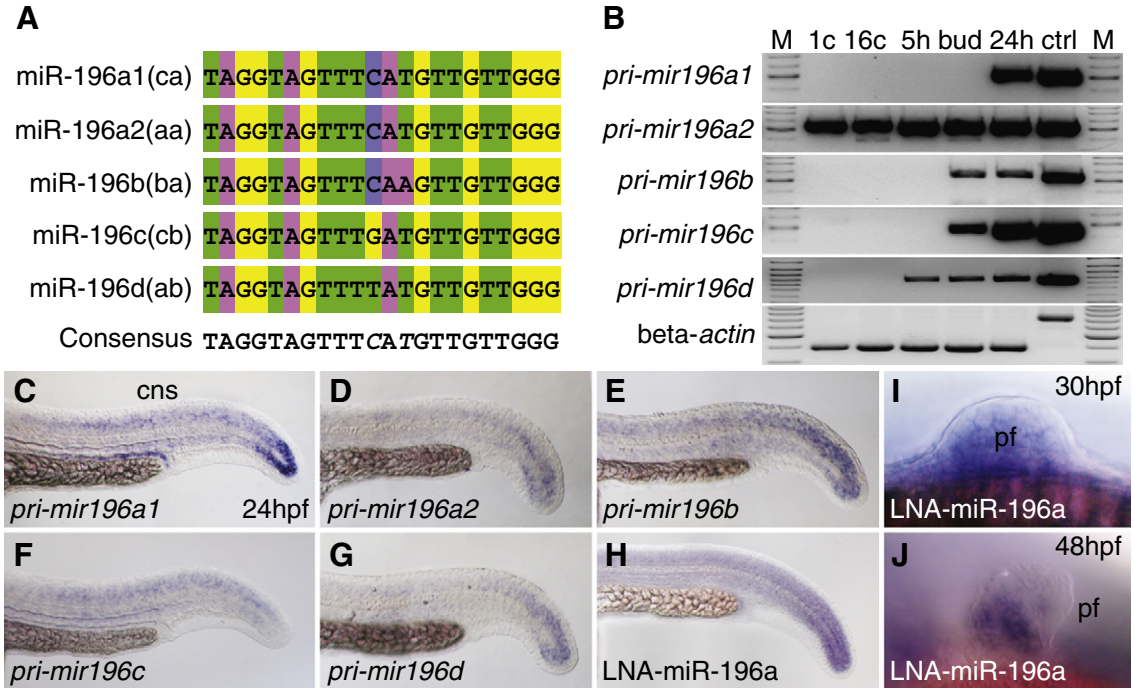

Fig. 1. Sequence and expression of *mir196* genes. (A) Alignment of mature miR-196 encoded by five *mir196* genes. (B) Expression of *mir196* paralogs studied by RT-PCR. Beta-*actin* (*bactin1*) was used as control for contaminating genomic DNA (ctrl lane). M, size marker; 1c, 1 cell stage; 16c, 16 cell stage; 5 h, 5 hpf (hours post-fertilization); bud, bud stage, about 10 hpf; 24 h, 24 hpf; ctrl, genomic DNA control. (C–H) Whole mount in situ hybridization for *mir196* primary transcripts showed expression in the tail bud and neural tube. (H) Linked nucleic acid (LNA) probe for miR-196a showed an expression pattern similar to the primary transcript. (I, J) LNA probes for miR-196a in the pectoral fin bud at 30 and 48 hpf. cns, central nerve system; pf, pectoral fin.

mir196 and hox targets

Sequence comparisons revealed that the 3′ UTRs of several zebrafish *hox cluster* genes surrounding *mir196* contain predicted miR-196 targets ((Yekta et al., 2008) and Supplementary Fig. S1A, Supplementary Table S1). The *mir196* genes lie between posterior *hox* paralogy groups 9 and 10, and ten *hox cluster* genes ranging from paralogy groups 5 to 13 contain predicted miR-196 binding sites. Conversely, *mir10* genes lie between anterior paralogy groups 4 and 5 and predicted targets are in anterior *hox* paralogy groups 1 to 4 and in *hoxd10a* (Supplementary Fig. S1A and Supplementary Table S1). This conserved non-random organization of *hox* cluster miRNA genes and their predicted targets suggests a conserved functional role between *hox* cluster genes and their neighboring miRNA genes (Yekta et al., 2008).

To test whether miR-196 regulates transcript levels of predicted *hox cluster* targets, we overexpressed miR-196 duplex or knocked down *mir196* expression with morpholino antisense oligonucleotide (Mo) designed to inhibit miR-196 maturation or control morpholino and then examined transcript levels by *in situ* hybridization in 24 hpf embryos using the hindbrain marker *egr2a* as internal control. Results showed that after overexpression of *mir196*, *hox* genes that have mismatch target sites and are expressed early in the region of the pectoral fin bud, including *hoxb5a*, *hoxb5b*, *hoxb6b* and *hoxc6a*, mostly retained their native expression level, but with a weakened anterior boundary (Supplementary Fig. S2A–L). Quantifying miR-196 by qPCR confirmed that overexpression elevated miR-196 levels 10–20 times normal and that knockdown resulted in 20% or less of normal miR-196 amounts, but that mis-matched miR-196 overexpression and control morpholino had no effect (Fig. S3A). We conclude that miR-196 can fine-tune the anterior expression border of *hoxb5a*, *hoxb5b*, *hoxb6b*, and *hoxc6a* either as direct targets or because they are downstream of a miR-196 target.

Zebrafish *hoxb8a* mRNA has a perfect target site for miR-196a like its ortholog *HOXB8* in human and mouse (Yekta et al., 2008). After overexpression of *mir196*, the level of *hoxb8a* transcript was diminished (Supplementary Fig. S2M–P). This result can be explained if *hoxb8a* transcript is degraded after miRNA binding like other transcripts with perfect matches between miRNAs and their target sites (Hornstein et al., 2005; Kawasaki and Taira, 2004; McGlinn et al., 2009; Yekta et al., 2004). To confirm the miR-196-related inhibition of *hoxb8a*, we made a reporter gene construct by attaching the 3′UTR of *hoxb8a* to the coding region of GFP (Supplementary Fig. S2Q). Results showed that co-injection of mRNA for the reporter with either miR-196a or miR-196b duplex inhibited fluorescence signal, and reciprocally, fluorescence increased after co-injection of the reporter mRNA and *mir196*-morpholino (Supplementary Fig. S2R–U). These results showed that both endogenous and injected miR-196 inhibit *hoxb8a* expression by degrading *hoxb8a* mRNA in zebrafish as in other species (Hornstein et al., 2005; Yekta et al., 2004).

miR-196 can block induction of zebrafish pectoral fin initiation

To learn the roles of miR-196 in embryonic development, we overexpressed miR-196 duplex by injection into early cleavage embryos and inhibited miR-196 processing and binding with morpholinos. Resulting animals survived to adulthood but showed highly specific phenotypes in the pectoral appendage, pharyngeal arches, and rostral vertebrae and ribs.

After miR-196 duplex injection, at least one pectoral fin was absent in 161 of 183 injected animals (Fig. 2A–G) and fin loss persisted into adulthood (Fig. 2H–J). At 5 dpf (days post-fertilization), the pectoral apparatus from 234 animals overexpressing miR-196 either lacked the endochondral disc and scapulocoracoid (42.3%, Fig. 2L), lacked the endochondral disc only (6.0%, Fig. 2M), or had normal fin buds (51.7%, Fig. 2N). The cleithrum, a dermal bone that does not form in fin mesenchyme (Mercader, 2007), was always present (Fig. 2K–N). We conclude that miR-196 blocks an early stage in pectoral fin development.

To learn how miR-196 acts to block pectoral fin formation, we interrogated steps in appendage development. In pectoral fin development (Fig. 3A), somite-derived retinoic acid (RA) acts on intermediate mesoderm to induce *wnt2ba*, which, along with RA acting via the retinoic acid receptor Rarab and *prdm1a* (Linville et al., 2009; Mercader et al., 2006), causes lateral plate mesoderm (LPM) to express *tbx5a* (Garrity et al., 2002), which turns on *fgf24* leading to expression of *fgf10a*, which activates the apical epidermal fold (AEF), thereby promoting fin bud outgrowth followed by the development of *lbx1b*-expressing fin muscle (Mercader, 2007; Wotton et al., 2008). To discover which step is sensitive to miR-196, we examined pectoral fin gene expression after *mir196* manipulation. miR-196-injected embryos lost expression of *lbx1b*, showing that miR-196 acts before fin muscle induction (Fig. 3B, C). Working backward through development, miR-196 injection blocked expression of *fgf10a*, *fgf24*, and *tbx5a*, the earliest expressed pectoral fin specific gene (Fig. 3D–I). Because *wnt2ba* is weakly expressed even in wild types (Koudijs et al., 2008; Mercader et al., 2006), it was difficult to detect whether its expression changed in the fin field region after miR-196 overexpression (data not shown). Expression of *prdm1a* is downstream of RA signaling in the pectoral fin bud (Mercader et al., 2006), and we found that miR-196 injection inhibited the expression of *prdm1a* in the pectoral fin field without affecting its expression in the CNS or pharyngeal arches (Fig. 3J, K), implying that miR-196 acts upstream of *prdm1a* in pectoral fin. RA induces *Hoxc6* expression in the mesenchyme of chick wing bud (Oliver et al., 1990) and we found that miR-196 injection inhibited the expression of *hoxc6a* in the pectoral fin field (Fig. 3L, M). This result is consistent either with the direct action of miR-196 on *hoxc6a* activity or an indirect action via retinoic acid signaling. The knockdown of miR-196 disrupted neither the expression of *fgf24* and *tbx5a* in the pectoral fin field (data not shown) nor the development of pectoral fins.

miR-196, fin buds, and retinoic acid signaling

Our gene expression analyses showed that the mechanism of action of miR-196 lies upstream of *prdm1a*, and hence pointed to a problem in RA signaling. To learn if *mir196* overexpression disrupts RA signaling, we utilized transgenic animals in which RA signaling activates a retinoic acid response element leading to expression of Yellow Fluorescent Protein (YFP) (Perz-Edwards et al., 2001) in the CNS by 43 hpf (Fig. 4A–D, left embryo). These reporter animals were injected with miR-196 duplex, or with mis-matched miR-196 duplex as control, or with miR-196 morpholino. Embryos overexpressing miR-196 displayed less fluorescence than controls, signifying reduced RA signaling (Fig. 4A, B, right embryo, Supplementary Fig. S4). Conversely, *mir196* knockdown gave elevated fluorescence compared to controls, and hence enhanced RA signaling (Fig. 4C, D, right embryo, Supplementary Fig. S4). These results demonstrate that miR-196 can inhibit RA signaling in the CNS, and, coupled with the fact that mutation of *aldh1a2*, which encodes an RA-synthesizing enzyme can delete the fin bud (Begemann et al., 2001), suggest the hypothesis that the pectoral fin phenotype of miR-196 overexpression results from decreased RA signaling.

The hypothesis that miR-196 negatively regulates RA signaling in fin bud initiation predicts that the inhibition of RA signaling by other methods should lead to the same phenotype. To test this prediction, we used DEAB, a reversible inhibitor of RA-synthesizing enzymes (Perz-Edwards et al., 2001). RA inhibition, like miR-196 overexpression (Fig. 2), caused a loss of pectoral fin outgrowth (Supplementary Fig. S5A–F) that persisted to adulthood (Supplementary Fig. S5G, H) and inhibited expression of *fgf24*, *tbx5a*, *fgf10a*, and *lbx1b* (Supplementary Fig. S5I–R). These results are as expected if miR-196 blocks fin bud development by inhibiting RA signaling.

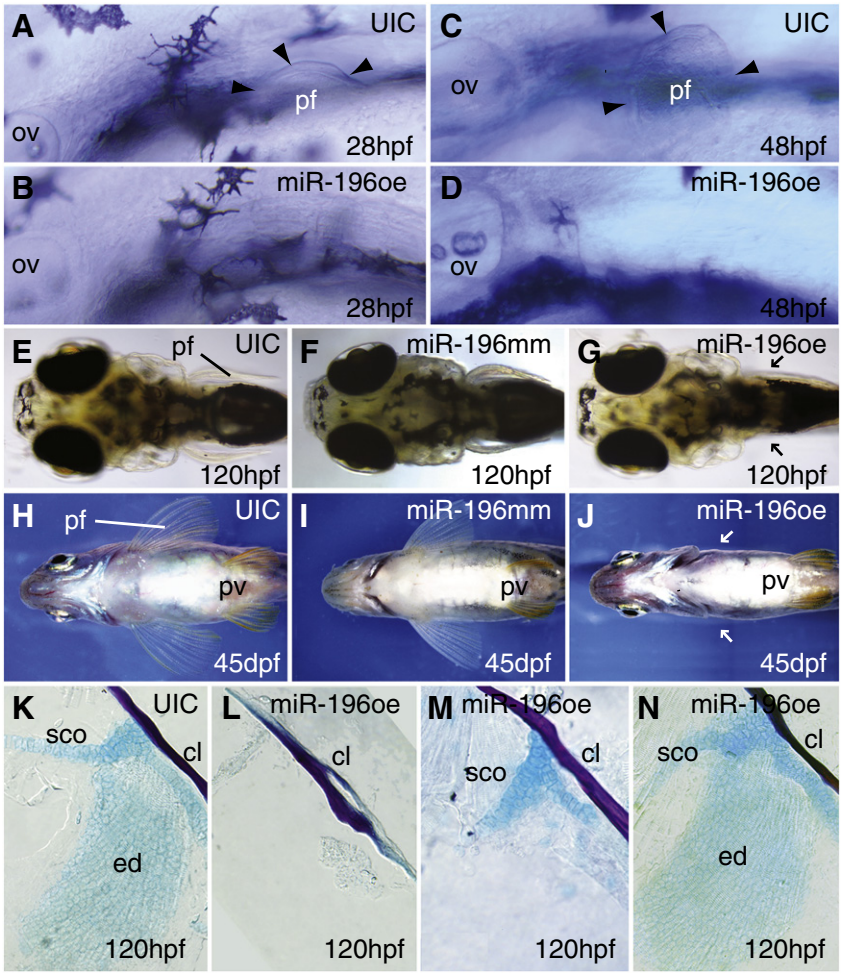

Fig. 2. miR-196 overexpression inhibits pectoral fin initiation. (A, C) Pectoral fin buds are readily detectable at 28 hpf and 48 hpf in normally developing uninjected control animals, but embryos overexpressing miR-196 (B, D) showed no evidence of a pectoral fin bud. Arrowheads mark the edges of pectoral fin buds. (E, F, H, I) Uninjected controls or miR-196 mismatch injected controls showed normal pectoral fins by 5 and 45 days post-fertilization (dpf), but larvae overexpressing miR-196 had not recovered pectoral fins by 5 dpf and became paraplegic adults (G, J, arrows point to missing pectoral fins). Pelvic fins were normal in fish with pectoral fin defects (J). (K–N) Dissected pectoral fins of 5 dpf larvae stained with Alcian blue for cartilage and Alizarin red for bone showed skeletal defects ranging from absence of the endochondral disc and scapulocoracoid (L, 42.3%, 234 total fins) to missing the endochondral disc but having part of scapulocoracoid (M, just 6%) to normal (N, 51.7%,). Abbreviations: cl, cleithrum; ed, endochondral disc; ov, otic vesicle; pf, pectoral fin or bud; pv, pelvic fin; sco, scapulocoracoid.

If miR-196 inhibits RA signaling, then excess RA should partially reverse this inhibition and rescue the fin phenotype of miR-196 overexpression; conversely, knockdown of endogenous miR-196 should partially relieve the inhibition of RA signaling and thus rescue a situation with diminished RA signaling. We increased RA signaling either by exposing 12 hpf embryos to synthetic RA (10^{-7} M) for 2 h or by reducing RA degradation using a mutation in *cyp26a1*, which encodes the enzyme that destroys RA (Emoto et al., 2005). At 120 hpf, both treatments resulted in short or absent pectoral fins (Grandel et al., 2002) (Supplementary Fig. S6A–F). In homozygous *cyp26a1*^{rw716} mutants, the endochondral disc was more sensitive than the scapulocoracoid (Supplementary Fig. S6G–J). While 89% (n = 63) of animals overexpressing miR-196 (5 nL) had no pectoral fin (Fig. 4E), only 48% of animals co-injected with miR-196 and treated with 10^{-7} M RA lacked pectoral fins (n = 81). Reciprocally, the knockdown of endogenous miR-196 partially rescued defective fins resulting from DEAB-inhibited RA signaling (Fig. 4F). We interpret this rescue to mean that with less endogenous miR-196, its target becomes more active, which partially overcomes diminished RA signaling caused by DEAB. These results show that not only injected miR-196, but also endogenous miR-196 inhibits pectoral fin bud initiation by interfering with RA signaling.

A target for miR-196 in fin bud development

To identify a molecular target related to RA signaling, we looked for potential miR-196 binding sites in the 3′UTRs of genes that are related to RA signaling, as well as genes known to be involved in pectoral fin initiation. A check of binding site prediction software (miRbase and MicroInspector (Rusinov et al., 2005)) showed that transcripts encoding Cyp26a1 and the retinoic acid receptor Rarab have predicted miR-196 target sites (Supplementary Fig. S6K and Fig. 6F, respectively), but other RA-pathway genes, including *aldh1a2*, all other *rar* and *rxr* genes, *prdm1a*, *fibin*, *tbx5a*, *wnt2b* and *fgf* ligands and receptor genes lacked such sites.

The target of miR-196 should possess at least three properties: knockdown of the target should (a) mimic the loss of fin bud initiation caused by miR-196 overexpression, (b) delete the pectoral fin bud expression domain of *tbx5a* as does miR-196 overexpression, and (c) lead to decreased RA signaling as we observed after miR-196 overexpression. A comparison of *cyp26a1* and *rarab* in these regards should suggest which is a better candidate as a miR-196 target. In *cyp26a1* mutants, the pectoral fin bud in zebrafish initiates and the animals form the scapulocoracoid (Supplementary Fig. S6G–J and (Emoto et al., 2005)), but after *rarab* knockdown and miR-196 overexpression, animals fail to initiate fin

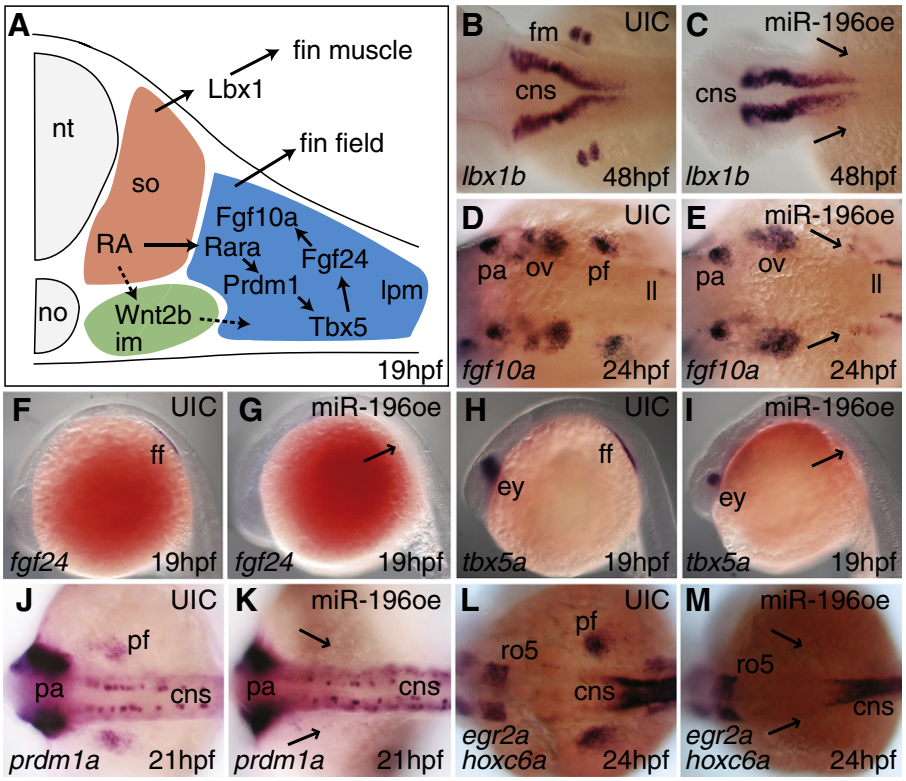

Fig. 3. miR-196 duplex injection inhibits expression of zebrafish fin development genes. (A) Model of the pectoral fin developmental pathway (after Mercader (2007)). In situ hybridization for *lbx1b* (B, C), *fgf10a* (D, E), *fgf24* (F, G), *tbx5a* (H, I), *prdm1a* (J, K), *hoxc6a* (L, M), on controls (B, D, F, H, J, L) and miR-196 overexpression (oe) animals (C, E, G, I, K, M) at ages indicated in the lower right of each panel. Arrowheads show the presumptive pectoral fin region in miR-196 duplex-injected animals. Results showed that miR-196 acts at or before the earliest stages of fin bud initiation. Abbreviations: cns, central neural system; ff, fin field; fm, pectoral fin muscle; im, intermediate mesoderm; ll, lateral line primordium; no, notochord; nt, neural tube; ov, otic vesicle; pa, pharyngeal arch; pf, pectoral fin bud; ro5, rhombomere 5.

bud development and become adults lacking pectoral fins (Fig. 4G–N and (Linville et al., 2009)). After *rarab* knockdown, pectoral fins either lacked the endochondral disc and scapulocoracoid or had normal fins (70% and 30%, respectively, n = 101). The expression domain of *tbx5a* is shifted anteriorly in *cyp26a1* mutants (Emoto et al., 2005) but in *rarab* knockdown and in miR-196 overexpression, we found that the *tbx5a* expression domain was deleted (Fig. 3H, I; Fig. 4O, P). Finally, inhibition of Cyp26a1, an RA degrading enzyme, augments RA signaling rather than reduces RA signaling as after *rarab* knockdown and *mir196* overexpression. Furthermore, overexpressing *rarab* by injecting *rarab* mRNA did not give a pectoral fin phenotype (data not shown), mimicking results for *mir196* knockdown. To further test whether Cyp26a1 is a target for miR-196 in pectoral fin initiation, we made a luciferase reporter construct by ligating the *cyp26a1* 3′UTR to the firefly luciferase coding region (Supplementary Fig. S6L). Co-transfection of tissue culture cells with this construct along with miR-196 showed that *cyp26a1* 3′UTR is insensitive to miR-196 (Supplementary Fig. S6M). These data make it unlikely that *cyp26a1* is the major miR-196 target relevant for the fin bud phenotype but are all consistent with *rarab* being the target.

If miR-196 attenuates *rarab*, then both *mir196* and *rarab* transcripts should be expressed in the same cells. Analysis showed that the expression of *rarab* (Hale et al., 2006; Linville et al., 2009) is similar to that of miR-196 in fin bud initiation (Fig. 5A–D, and shown in two-color double in situ hybridizations in Supplementary Fig. S7, along with double in situs of *rarab* and *tbx5a*). To see if miR-196 could target the *rarab* 3′UTR, we used a firefly luciferase assay in cultured cells using *Renilla* luciferase as an internal standard. We attached the *rarab* 3′UTR with its three predicted miR-196 binding sites to luciferase coding sequence (Fig. 5E, F) and co-transfected this construct and miR-196 into human 293 T cells. miR-196 led to reduced luciferase fluorescence from the *rarab* 3′UTR construct compared to the control (Fig. 5G), showing that miR-196 can act on the *rarab* 3′UTR to inhibit message stability and/or translation. To test this interaction in living embryos, we co-injected a construct containing the GFP coding region followed by the *rarab* 3′UTR (Fig. 5E) and then overexpressed or knocked down miR-196. Embryos injected with miR-196 had less GFP fluorescence than uninjected controls or controls injected with miR-196 mismatch duplex, but embryos experiencing miR-196 knockdown had more fluorescence than controls (Fig. 5H–K, Supplementary Fig. S8). Deletion of the three predicted binding sites for miR-196 in the *rarab* 3′UTR led to no significant difference in GFP fluorescence compared to controls (Fig. 5L–O). This reporter assay confirmed direct interaction between miR-196 and the *rarab* 3′UTR in living embryos. We conclude that *rarab* is the miR-196 target responsible for the pectoral fin initiation phenotype. Because miR-196 overexpression or knockdown did not change the amount of *rarab* transcript (Supplementary Fig. S9), miR-196 is likely to act more strongly on *rarab* translation than on message stability. To determine whether miR-196 is itself a target of RA signaling, we treated animals with RA or with DEAB, an inhibitor of RA synthesis, and measured levels of miR-196 by qPCR. Results showed that, relative to untreated controls and DMSO carrier treated controls, RA treatments slightly decreased miR-196 levels and RA knockdown increased miR-196 levels to a small degree (Fig. S3B). We conclude that, if there is an effect of RA on miR-196 levels, it is in the direction of RA down-regulating miR-196 expression, but the effect is not strong.

mir196 inhibits branchial arch segmentation

Animals overexpressing *mir196* lacked not only pectoral fins, but also lacked one, and only one, pharyngeal arch (PA). Zebrafish have seven PAs, including mandibular (PA1), hyoid (PA2), and five branchial (gill) arches (PA3-7). After miR-196 overexpression, PA1

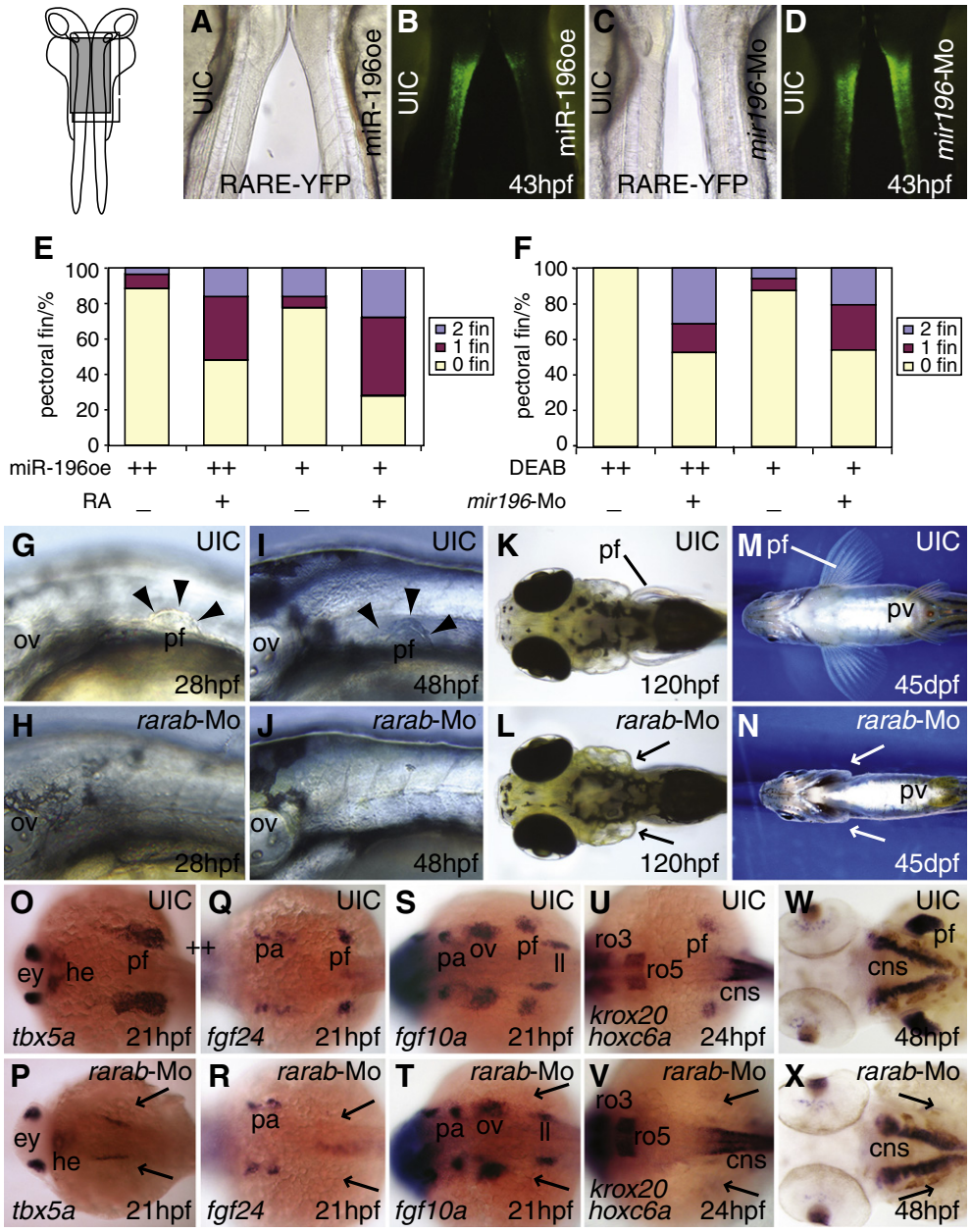

Fig. 4. miR-196 activity modulates RA signaling. (A) Bright field microscopy of a 43 hpf uninjected control transgenic RA signaling reporter individual and a miR-196 injected 43 hpf RA-reporter embryo oriented back-to-back as in the insert at the left of part (A), with the boxed region blown up in A–D. (B) The animals in (A) was viewed in fluorescence microscopy. The intensity of green fluorescence is proportional to the level of RA signaling, and was greatly reduced after miR-196 overexpression. (C) Bright field and (D) fluorescence views of a control (left) and a miR-196-morpholino injected 43 hpf embryo (right). The elevated expression of YFP found after miR-196 knockdown is opposite to the phenotype found after miR-196 overexpression. (E, F) Rescue experiments. (E) Although injecting cleavage embryos with 5 nL of miR-196 duplex and treating them with DMSO as controls (++) caused a greater fraction of animals to develop without pectoral fins (89%, n = 63) than injections with 1 nL (+) (78%, n = 76), both can be rescued by RA treatment (+) (48%, n = 81 and 28% n = 61 without fin respectively). This experiment was repeated four times. (F) Treating embryos with 1×10^{-5} M (++) or 5×10^{-6} M (+) DEAB to decrease RA levels resulted in all (100%, n = 31) or most of the animals (87.5%, n = 16) lacking pectoral fins respectively, but first injecting cleavage embryos with 1 nL of 3 mM *mir196*-Mo (+) to diminish the inhibition of RA signaling before treating embryos with DEAB, led to partial rescue of the fin phenotype (just 53%, n = 51 or 54%, n = 48, respectively). Compared to controls (G, I, K, M), *rarab*-Mo injection (H, J, L, N) inhibited pectoral fin outgrowth already by 28 hpf (G, H) and this phenotype was maintained through 48 hpf (I, J), 120 hpf (K, L), and into adulthood (M, N) verifying the specificity of the effect. Arrowheads mark the edge of the pectoral fin and arrows direct attention to missing pectoral fins and buds. (O–V) *rarab*-Mo inhibited expression of the pectoral fin genes *tbx5a* (O, P), *fgf24* (Q, R), *fgf10a* (S, T), and *hoxc6a* (U, V), as well as the fin muscle marker gene *lbx1b* (W, X) specifically in the fin field region while leaving other expression domains intact, the same result as from miR-196 injection. Arrows: missing pectoral fin buds. cns, central neural system; ey, eye; he, heart; im, intermediate mesoderm; ll, lateral line primordium; ov, otic vesicle; pa, pharyngeal arch; pf, pectoral fin; pv, pelvic fin; ro3, -5, rhombomere3, -5.

and PA2, as well as the tooth-bearing PA7, were normal. In 84% (n = 254) of miR-196 duplex-injected animals, however, one or both sides of the animal had four rather than five branchial arches (Fig. 6A, B). PA3 to PA5 were always normal in morphology, but occasionally a short PA6 was fused to PA7 after miR-196 overexpression (Fig. 6B, insert). This malformation suggests that the missing arch was PA6. This result shows that overexpression or ectopic expression of *mir196* is sufficient to reduce the number of branchial arch segments. We infer that miR-196 inhibits a process necessary to add branchial arches, probably PA6.

To distinguish between the hypotheses that the loss of PA6 arises from overexpression or ectopic expression of miR-196, we knocked down miR-196 with a morpholino designed to inhibit miRNA processing. Results showed that 33% of injected animals (n = 140) had six

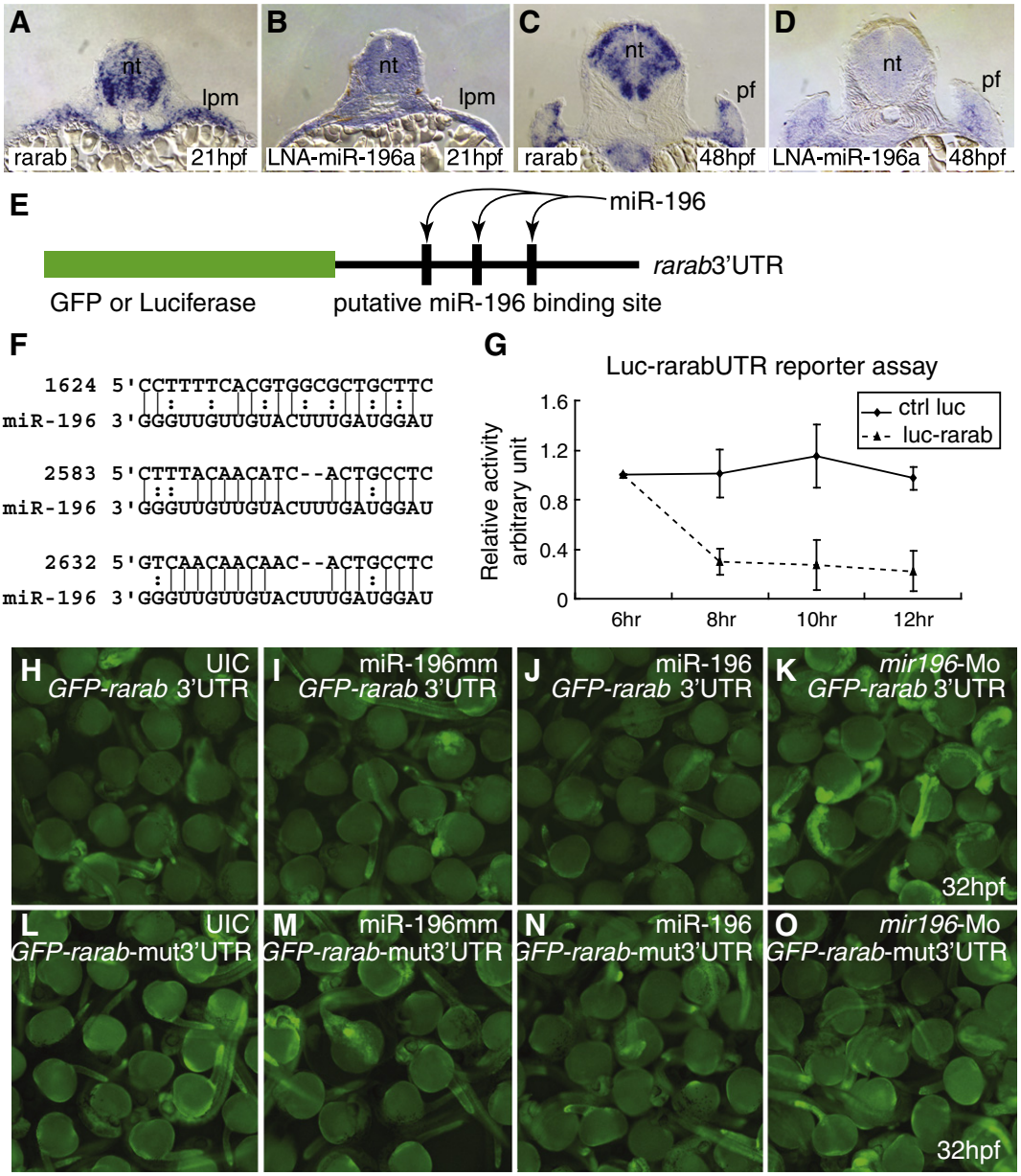

Fig. 5. *rarab* is a target of miR-196. (A–D) In situ hybridization on tissue sections for *rarab* (A, C) and miR-196 (using LNA probe, B, D) at 21 hpf (A, B) and 48 hpf (C, D) shows that *rarab* and miR-196 are co-expressed in the lateral plate mesoderm at 21 hpf (A, B) and medially in the pectoral fin bud at 48 hpf (C, D). (E–O) Reporter assays. (E) Reporter assay constructs used luciferase in (G) and GFP in (H–K). (F) The 3′UTR of *rarab* has three predicted binding sites for miR-196 (nucleotide position according to NM_131399, binding sites were retrieved or predicted from miRBase.com and MicroInspector). (G) miR-196 can interfere with expression of a luciferase reporter construct bearing the 3′UTR of *rarab* compared to control. This experiment was repeated three times. (H–K) GFP-*rarab* 3′UTR mRNA was injected into early cleavage stage embryos either by itself (H) or co-injected with miR-196 mismatch (I), with miR-196 duplex (J), or with *mir196*-Mo (K). miR-196 depressed fluorescence but *mir196* knockdown enhanced fluorescence, as predicted by the hypothesis that miR-196 acts directly on the 3′UTR of *rarab*. This experiment was repeated four times. (L–O) The three predicted miR-196 binding sites were removed from the GFP-*rarab* 3′UTR construct to make a GFP-*rarab*-mut3′UTR. GFP-*rarab* mut3′UTR mRNA was injected into early cleavage stage embryos either by itself (L) or co-injected with miR-196 mismatch (M), with miR-196 duplex (N), or with *mir196*-Mo (O). miR-196 did not depress fluorescence (N) and *mir196* knockdown did not enhance fluorescence (O) from this mutant construct. This experiment was repeated three times. lpm; lateral plate mesoderm; pf, pectoral fin bud.

rather than the normal five branchial arches (Fig. 6C). Some animals with five branchial arches had an additional skeletal element fused to PA7, suggesting that endogenous miR-196 normally inhibits the arch just anterior to PA7. This result shows that endogenous miR-196 is necessary to prevent the addition of supernumerary branchial arches. Because the miR-196 knockdown phenotype is opposite to that of miR-196 overexpression, we conclude that precisely adjusted levels of miR-196 are required for proper branchial arch segmentation.

Cartilage-forming cells in pharyngeal arches arise from post-migratory neural crest that is divided into several streams by endodermal pouches (Fig. 6D and Crump et al. (2004)). To determine whether miR-196 acts primarily on the endodermal pouches or only on the neural crest, we used transgenic *fli*-GFP fish in which the skeletogenic crest fluoresces green (Lawson and Weinstein, 2002) and then stained animals with the antibody zn-8 as a marker for pharyngeal endoderm (Trevarrow et al., 1990). In contrast to normal 36 hpf embryos with seven pharyngeal arches (Fig. 6D), *mir196* overexpression embryos lacked one endodermal pouch (Fig. 6E). Conversely, *mir196* knockdown embryos had an extra endodermal pouch that resulted in an extra pharyngeal arch precursor (Fig. 6F). These result in embryos that correspond to the cartilage phenotype of miR-196 manipulated larvae and support the hypothesis that miR-196 derived defects in pharyngeal

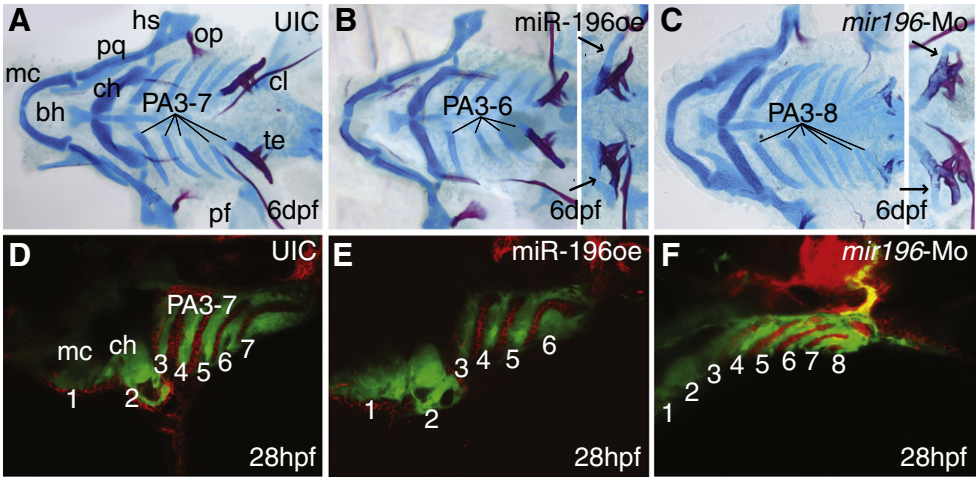

Fig. 6. miR-196 regulates pharyngeal arch segmentation via pharyngeal endoderm. (A–C) Zebrafish embryos injected with miR-196 duplex or *mir196*-Mo were raised to 6 dpf and stained with Alcian blue for cartilage and Alizarin red for bone. (A) Control larvae had seven pharyngeal arches, including Meckels and ceratohyal cartilages (in PA1 and PA2) and five branchial arches (in PA3–7). (B) Animals overexpressing miR-196 lacked one branchial arch. Some animals with four branchial arches (insert) possessed a skeletal element attached to the last arch (arrows), suggesting that the missing arch was the one anterior to the tooth-bearing pharyngeal arch-7. (C) Injection of *mir196*-Mo resulted in animals with extra branchial arches. Some animals with seven pharyngeal arches (insert) displayed extra skeletal elements attached to pharyngeal arch-7 (arrows), suggesting that the extra arch was the one just anterior to PA7. (D–F) Transgenic animals expressing GFP in the neural crest (green) that were either overexpressing (E) or knocked down (F) for miR-196 showed defective segmentation of endodermal pouches stained with zn-8 antibody (red) and pharyngeal arches (green) consistent with observed alterations in arch numbers. Abbreviations: bh, basihyal; ch, ceratohyal; cl, cleithrum; hs, hyosymplectic; mc, Meckels cartilage; op, opercle; pa, pharyngeal arch; pf, pectoral fin; pq, palatoquadrate; te, teeth.

arch patterning arise from initial effects on the patterning of pharyngeal pouch endoderm. Together, these results lead to the conclusion that *mir196* acts in pharyngeal arch endoderm to suppress the formation of a posterior pharyngeal pouch.

Normal miR-196 levels are essential to pattern the axial skeleton

Controlled levels of miR-196 are important for proper segmentation not only of branchial arches but also of the rostral axial skeleton. The anterior four vertebrae of zebrafish and other Otophysi form the Weberian apparatus, bones that transmit sound from the swim bladder to the inner ear (Grande and Young, 2005). Caudal to the Weberian apparatus, normal animals have about ten rib-bearing precaudal vertebrae (Fig. 7A, D and Bird and Mabee (2003)). Adult fish developing from embryos injected with miR-196 duplex showed disrupted rostral axial skeletons, including axial shifts in the patterning of the Weberian apparatus and fewer precaudal vertebrae and ribs (Fig. 7B, D, E–L). Adult fish developing from embryos injected with miR-196 Mo did not show defects in the Weberian apparatus but they had more ribs and rib-bearing precaudal vertebrae than normal (Fig. 7C, D). Statistically, miR-196 injected animals had on average 0.7 fewer segments in the Weberian apparatus than wild types (73.2% of 56 injected animals were affected), and 2.5 fewer ribs (81.8% affected), and 2.1 fewer rib-bearing precaudal vertebrae than normal (36.2% affected) (Fig. 7D).

In wild-type fish, the Weberian apparatus has four highly modified vertebrae, each with bone and cartilage morphologies that specify their identity (Fig. 7E, F, I, J). The lateral process-1 (lp1), -2 (lp2), the intercalarium (in), the tripus bones (tr), the neural arch-3 (na3), neural arch-4 (na4), the highly modified rib-4 (r4) ,os suspensorium (os), supranueral-3 (sn3), and -4 (sn4) are attached to one of the four vertebra in the Weberian apparatus. Analysis of these skeletal structures showed that the overexpression of miR-196 provoked fate transformations in the Weberian apparatus. For example, in the animal in Fig. 8G, the second segment (segment #2) had the joint for the intercalarium, which is appropriate for a normal vertebra-2, but this segment possessed a dorsal projection that appeared similar to, but not as broad as, neural arch-3 (asterisk in Fig. 7G). The morphology of this animal's segment #3 was similar to the normal v4 with a neural arch-4 and rib-4 like rib (arrow in Fig. 7G). Segment #4 had a rib appropriate for v5 (arrowhead in Fig. 7G). We conclude that in this fish, the identity of segments #2–4 were partially transformed into more posterior fates, an apparent homeotic transformation. Alternatively, v2 or v3 was deleted and segment #2 assumed an identity intermediate between v2 and v3. The animal in Fig. 7H had a normal v1 with a normal lateral process-1, but segment #2 had an abnormally short lateral process-2; segment #3 had a ventral projection intermediate in character between the tripus (Fig. 7E, F) and anteriorly projecting, forked rib-4 (r4) which is more appropriate for the next segment more posterior (arrow in Fig. 7H), and a neural arch more similar to neural arch-4 than neural arch-3; in addition, segment #4 had a rib with the morphology of rib-5 rather than rib-4 (arrowhead in Fig. 7H). Fig. 7K is a ventral view of the Weberian apparatus of an animal overexpressing miR-196 with relatively normal v1 and v2, but v3 showed partial posterior transformation on the right side with a forked tripus anteriorly oriented like rib-4, although the left side was relatively normal; segment #4 had a rib on the left side that was appropriate for rib-4, but on the right side, the rib pointed backwards and was not forked, which are characteristics of the more posterior rib-5. The Weberian apparatus of the animal in Fig. 7L had a segment #2 with a normal tripus on the right side (rather than on the normal v3) and a malformed tripus on the left side; segment #3 of this animal had a DEL id="del105" orig="n"; rib-4-like structure on the right side and a nearly normal tripus on the left side (arrows in Fig. 7L); segment #4 on both sides had ribs appropriate for rib-5 (arrowheads in Fig. 7L). This phenotype occurred repeatedly in affected animals (see supplementary Table S2). In summary, analysis of miR-196 overexpression animals suggests that the identities of rostral vertebrae are transformed into structures appropriate for more posterior elements.

In contrast to the overexpression results, in which the Weberian apparatus showed posterior phenotypes and fewer than normal ribs, knockdown of miR-196 resulted in fish that had a morphologically normal Weberian apparatus but tended to have extra ribs and extra rib-bearing precaudal vertebrae (Fig. 7C, D). This result shows that native miR-196 expression levels are important for axial segment morphology. With regard to rib and precaudal vertebrae number, the results from miR-196 knockdown (segment gain) were opposite that of miR-196 overexpression (segment loss). In summary, the manipulation of miR-196 levels resulted in altered numbers and homeotic-like fate transformations and segmentation abnormalities along the axial skeletal system.

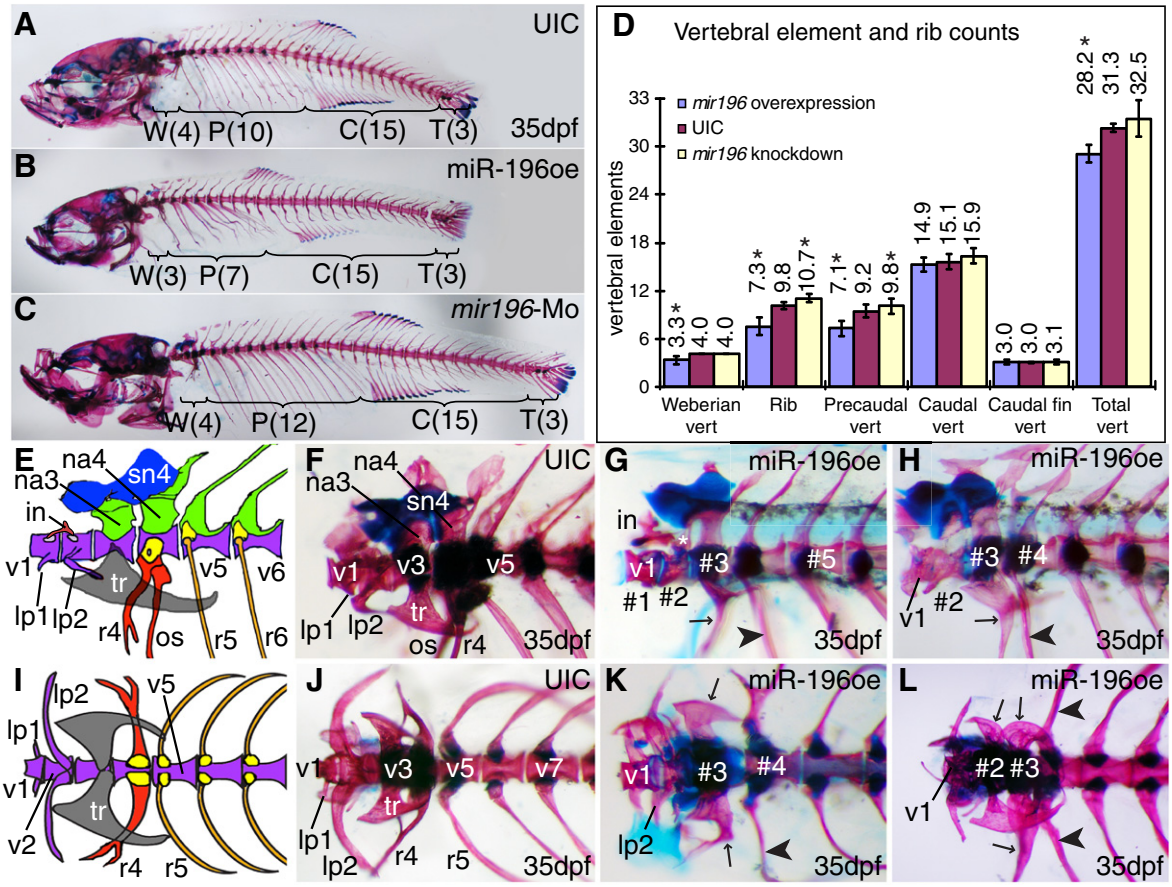

Fig. 7. Over- and under-expression of miR-196 disrupts patterning of the axial skeleton. (A) Normal axial skeleton stained for cartilage (Alcian blue) and bone (Alizarin red) showing 4, 10, 15 and 3 vertebrae in the Weberian apparatus (region W), rib-bearing precaudal vertebra (region P), caudal vertebra (region C) and caudal fin vertebra (region T), respectively. (B, D) Overexpression of *mir196* showing deletion of one Weberian vertebra and three ribs with their precaudal vertebrae. (C, D) Morpholino knockdown of miR-196 resulted in extra ribs and extra rib-bearing precaudal vertebrae. (D) Skeletal element counts after miR-196 manipulation showing reciprocal effects of overexpression and knockdown in the rostral axial skeleton. Asterisks indicate statistical significance compared to UIC (uninjected control) (Student *T*-test, $p<0.001$). UIC, n = 79; miR-196oe (overexpression), n = 56; *mir196*-Mo (miR-196 knockdown), n = 122. (E, F, I, J) Weberian apparatus sketch (after (Grande and Young, 2005)) and skeleton staining, lateral and dorsal views, respectively. (G, H, K, L) Overexpression of miR-196, lateral (G, H) and ventral (K, L) views of the Weberian apparatus from four different individuals. In wild-type fish, the Weberian apparatus has four highly modified vertebrae, each with bone and cartilage morphologies that specify their identity (E, F, I, J). Typically, the first vertebra (v1) has a pair of anterior-laterally projecting bones called the lateral process-1 (lp1) and dorsally, a small bone called intercalarium (in) that contacts with vertebra-2 (v2). V2 normally has a pair of laterally projecting bones (the lateral process-2, lp2) on each side. Lp2 is larger than lp1 (E, I). Vertebra-3 (v3) has a pair of lateral tripus (tr) bones, a triangular shaped bone, and neural arch-3 (na3) dorsally. Vertebra-4 (v4) has a pair of highly modified ribs (r4) protruding ventral-laterally that bears os suspensorium bones ventrally and dorsally, a neural arch-4, on top of which, supranueral-4 (sn4) usually fuses anteriorly with supranueral-3 (sn3) on v3. Precaudal vertebrae are defined by their parapophyses, which support ribs, and their lack of hemal arches and hemal spines, which are found on v15-v28 (Bird and Mabee, 2003). Treated animals are discussed in the text. Abbreviations: #1, #2, #3, vertebrae numbers from anterior without regard to identity; in, intercalarium; lp1, lp2, lateral processes; na3, na4, neural arches; os, os suspensorium; r4, r5, ribs; tr, tripus; v1, v2, v3, v4, v5, v7 vertebrae with identities.

Axial skeletal segmentation depends on early somitogenesis (Bagnall et al., 1988) (Morin-Kensicki et al., 2002) (Sparrow et al., 2007). To understand how miR-196 regulates axial skeleton segmentation, we scored larval somite numbers after miR-196 overexpression or knockdown (Supplementary Fig. S10). By 4 dpf, wild-type zebrafish embryos had developed about 30 or 31 somites (78.4%, n = 74). We found that overexpression of miR196 reduced total somite number (81.1% of 53 animals had fewer than 30 somites), while knockdown of *mir196* induced more somites than control fish (62.1% of 66 animals had more than 31 somites). This result is consistent with our counts of ribs and vertebrae in adults, and shows that miR-196 regulates somitogenesis.

Discussion

Overexpressing miR-196 caused four highly specific phenotypes—failure of pectoral appendage initiation, deletion of one pharyngeal arch, transformation of vertebral identity and number, and change in somite number.

The interaction of hox cluster protein-coding genes and mir196 genes

The similar expression patterns of miR-196 genes and their neighboring *hox* cluster protein-coding genes would be expected if they share regulatory mechanisms (Yekta et al., 2008). *Hox* cluster protein-coding genes are rich in miR-196 targets in zebrafish as they are in tetrapods (Yekta et al., 2008). Like its tetrapod ortholog, zebrafish *hoxb8a* is has a site with perfect complementarity to miR-196 and our results showed that in zebrafish, as in tetrapods, miR-196 acts on *hoxb8a* expression by decreasing messenger stability. Other predicted *hox* cluster target genes for miR-196 have only partially complementary matches with miR-196, suggesting that miR-196 does not regulate these genes by message degradation. We observed changes in transcript distribution for *hoxb5a*, *hoxb5b*, *hoxb6b* and *hoxc6a* at their anterior expression borders, suggesting that miR-196 may regulate a factor upstream of these *hox* cluster protein-coding genes. Mutations in genes that encode retinoic acid synthesizing or degrading enzymes (*raldh1a2* or *cyp26a1*, respectively) (Begemann et al., 2001; Emoto et al., 2005) shift the anterior border of *hox* cluster

protein-coding genes, with up-regulation of RA signaling causing rostral expansion, implying that the phenotype we saw may be a combination of direct control (miR-196 binds and inhibits translation of *hox* target genes) and indirect regulation (miR-196 regulates RA signaling, which secondarily regulates *hox* gene expression); alternatively, miR-196 may regulate these *hox* cluster protein-coding genes by an unknown regulatory mechanism.

miR-196 inhibits pectoral fin induction by inhibiting rarab expression

Animals injected with miR-196 duplex lacked pectoral fins and showed diminished expressions of even the earliest fin bud markers. We conclude that miR-196 overexpression inhibits the initiation, rather than the patterning or elongation of pectoral fin buds. No conclusions can be drawn with respect to the effect of miR-196 on the pelvic fin bud because it develops more than 2 weeks after fertilization (Grandel et al., 2002), which is long after the injected miRNA would be effective. Other miRNAs are involved in zebrafish fin regeneration (Thatcher et al., 2008). Retinoic acid signaling acts upstream of pectoral appendage initiation (Gibert et al., 2006; Grandel et al., 2002; Linville et al., 2009; Mercader et al., 2006; Waxman et al., 2008). Because we found that miR-196 knockdown partially rescued diminished RA signaling, we conclude that endogenous miR-196 plays a role in normally developing zebrafish. Transcript from *rarab* appears in both the CNS and lateral plate mesoderm (Hale et al., 2006; Linville et al., 2009) and contains three predicted partially complementary binding sites for miR-196, suggesting the hypothesis that miR-196 attenuates RA signaling by lowering levels of Rarab protein production. Furthermore, *rarab* knockdown blocks pectoral appendage initiation (Linville et al., 2009), which would be expected if miR-196 inhibits pectoral fin initiation by limiting *rarab* function. Likewise, miR-196 overexpression diminished RA signaling in the CNS as detected in the RARE-YFP transgenic line, and the same result was obtained in the same line after direct *rarab* knockdown (Linville et al., 2009). Finally, a luciferase assay in tissue culture cells and a GFP assay in living embryos both showed that miR-196 functions via the 3′UTR of *rarab*. Because miR-196 overexpression does not inhibit the accumulation of significant quantities of *rarab* transcript and similar experiments showed a substantial decrease of transcript levels for *hoxb8a*, which serves as a positive control, we conclude that miR-196 acts more on translation than on message stability to modulate expression of *rarab*. These results are as predicted by the hypothesis that miR-196 overexpression blocks fin bud initiation, at least partially, by binding the *rarab* 3′UTR in lateral plate mesoderm to inhibit its translation, thereby diminishing the ability of lateral plate cells to detect somite-derived RA, which leads to lack of *tbx5a* induction, without which the fin bud cannot initiate. Although miR-196 morpholino knockdown did not give a pectoral fin bud phenotype in otherwise normal development, evidence that endogenous miR-196 is involved in pectoral fin bud initiation comes from the demonstration that miR-196 knockdown rescued diminished RA signaling. Thus, we conclude that *rarab* is a target of miR-196 for pectoral fin bud initiation in zebrafish.

Tetrapods have three *Rar* genes (*Rara*, *Rarb*, *Rarg*), and zebrafish has duplicate copies of *Rara* and *Rarg* but no *Rarb* gene (Hale et al., 2006). The functions of the three tetrapod *Rar* genes appear to have partitioned among the four zebrafish *raraa*, *rarab*, *rarga* and *rargb* genes (Linville et al., 2009). As in zebrafish, pectoral appendage initiation in mouse requires RA signaling (Niederreither et al., 1999), and double knockout of *Rara* and *Rarg* in mouse causes hypoplastic pectoral limb buds (Wendling et al., 2001). Thus, the mechanism of pectoral appendage initiation is generally conserved between zebrafish and tetrapods, but because none of the *Rar* or *Rxr* genes in mouse, human, or chicken have predicted miR-196 targets, the role of miR-196 may differ in zebrafish and tetrapods.

Although several *hox* genes that are expressed in pectoral fins have predicted miR-196 binding sites, they are unlikely to be responsible for the fin bud phenotype because most are expressed downstream of RA signaling in the fin bud and their temporal–spatial expression patterns exclude them from functioning during pectoral fin bud induction. For example, although *hoxb5b* is an RA-responsive gene expressed in the forelimb field, its function is dispensable for forelimb formation (Waxman et al., 2008). Furthermore, although miR-196 causes a decrease in *hoxb8a* message levels in zebrafish as in tetrapods (Kawasaki and Taira, 2004; McGlinn et al., 2009; Yekta et al., 2004), *hoxb8a* is unlikely to be the gene responsible for miR-196 regulation of pectoral fin bud initiation because (1) it is expressed in zebrafish pectoral fin buds well after initiation, (2) because our experiments showed that *hoxb8a* knockdown in zebrafish does not affect pectoral fin development (data not shown), and (3) because *hoxb8a* mutants in medaka initiate fin bud development normally but are defective in the maintenance of pectoral fin bud outgrowth (Sakaguchi et al., 2006). In addition, we used morpholinos to knockdown individually the expression of *hoxb5a*, *hoxb5b*, *hoxb6b*, *hoxc6a* and none of them showed pectoral fin defects (data not shown). Thus none of the five *hox* genes we checked are required for pectoral fin initiation. We conclude that miR-196 regulates pectoral fin bud initiation primarily by inhibiting *rarab* expression.

miR-196 and pharyngeal arch patterning

Overexpression experiments showed that miR-196 inhibits the formation of a posterior arch, probably PA6, and knockdown experiments showed that this mechanism applies to endogenous miR-196 as well. In principle, miR-196 could perform this role by modulating either *hox* gene expression, RA signaling, or FGF signaling. In mouse, *Hox2* paralogs help control PA2 and PA1 identity (Minoux et al., 2009) and *Hox3* paralogs help specify PA3 and PA4 (Minoux et al., 2009), but the mechanisms that control the identity of PA5 to PA7 are as yet unclear. In zebrafish, *hoxb5a* is expressed strongly and *hoxb5b* weakly in PA3–7 (Bruce et al., 2001; Jarinova et al., 2008), suggesting that *Hox5* paralogs could help pattern posterior arches. Although *hoxb5a* and *hoxb5b* are both predicted miR-196 targets, are both expressed in the posterior PAs, and our experiments show that both are sensitive to miR-196, the knockdown of *hoxb5a* and *hoxb5b* in zebrafish and *Hoxb5* in mouse is not reported to give an arch phenotype (McIntyre et al., 2007; Waxman et al., 2008) (and our unpublished experiments). These considerations make it unlikely that *hoxb5* genes are the miR-196 targets responsible for the arch phenotype.

Because retinoic acid is a posteriorizing factor in pharyngeal endoderm (Bayha et al., 2009) and suppression of RA signaling deletes branchial arches (Begemann et al., 2001; Birkholz et al., 2009), it is possible that miR-196 acts on pharyngeal endoderm to inhibit RA signaling. The rather broad and general phenotype arches after the manipulation of RA signaling, however, contrasts with the highly specific effect of miR-196 overexpression. Inhibiting RA signaling progressively between 16 and 30 hpf results in fewer deleted PAs (Kopinke et al., 2006), suggesting that, if miR-196 acts through RA signaling to suppress PA6, it must act at or after 30 hpf. Double knockout of *Rara* and *Rarb* alters development of posterior PAs in mouse (Dupe et al., 1999) in ways that mimic miR-196 overexpression in zebrafish. These considerations suggest that pharyngeal phenotypes of miR-196 manipulated zebrafish might, like the fin phenotype, be mediated by *rarab*. Although *rarab* is expressed in PAs (Hale et al., 2006; Linville et al., 2009), *rarab* morpholino knockdown had no effect on the branchial arch phenotype ((Linville et al., 2009) and our unpublished data). In contrast, knockdown of *rarga*, which did not predict miR-196 binding sites, did alter gill arch formation (Linville et al., 2009). Thus, either *rarab* inhibition does not explain the gill arch phenotype of miR-196 manipulation, or the knockdown of *rarab* activity by miR-196 overexpression is more profound than *rarab*

knockdown by morpholino. The endoderm of the pharyngeal arches expresses *cyp26a1* and the *cyp26a1* 3′UTR has miR-196 binding sites, but PA3-7 are normal in *cyp26a1* mutants (Emoto et al., 2005), thus ruling out *cyp26a1* as the miR-196 target responsible for the arch phenotype. Thus, in pharyngeal arches, miR-196 appears likely to act either on a component of the pharyngeal segmentation mechanism or on an as yet unknown gene essential for the specification of PA6.

Mesoderm- and CNS-derived Fgf3 and Fgf8 help direct the segmentation of pharyngeal pouches (Crump et al., 2004), suggesting that miR-196 may alter Fgf signaling. Our finding that manipulating miR-196 levels alters RA signaling in the hindbrain could lead to alterations in Fgf signaling that promote the loss or gain of PA6. Again, however, the great specificity of the miR-196 phenotype contrasts to the broader perturbation of PA3-7 development caused by Fgf manipulations, and suggests that, if miR-196 acts on Fgf signaling, it must be through a tissue-specific downstream target of Fgf because none of the zebrafish *fgf*, *fgfr* and other Fgf pathway genes have predicted miR-196 binding sites.

These considerations lead us to propose that in normal development, miR-196 attenuates action of a gene essential to direct the formation of pharyngeal pouches between PA5 and PA7. The identity of this target is as yet unknown.

miR-196 and axial skeleton patterning

Manipulating miR-196 levels provoked patterning anomalies specifically in regions of the axial skeleton that express *hox* genes with predicted miR-196 targets. The predicted miR-196 target *hoxb5a* is expressed in somites-2 and -3 but the target *hoxb5b* is not expressed in the somites (Bruce et al., 2001; Jarinova et al., 2008). Somites-1 and -2 and the anterior of somite-3 do not contribute to vertebrae in zebrafish or tetrapods, but in tetrapods at least, they contribute to the caudal part of the skull (Huang et al., 2000; Morin-Kensicki et al., 2002), which was morphologically normal in zebrafish over- or under-expressing miR-196. Furthermore, altered patterning of the zebrafish axial skeleton is not seen after knockdown of *hoxb5a* or *hoxb5b* ((Waxman et al., 2008), confirmed in our unpublished experiments). In mouse, *Hoxb5* mutants show an anteriorizing homeotic transformation of the caudal cervical and first thoracic (rib-bearing) vertebrae (Rancourt et al., 1995); while, conversely, we observed a posteriorizing effect in the homologous vertebrae after miR-196 overexpression. This result argues against the hypothesis that miR-196 acts on *hoxb5a* or *hoxb5b* to regulate anterior axial skeleton patterning.

Five predicted miR-196 targets (*hoxb6b*, *hoxc6a*, *hoxb8a*, *hoxb8b* and *hoxc8a*) are expressed with anterior borders in somites-3 to -7, which form the Weberian apparatus (Bruce et al., 2001; Morin-Kensicki et al., 2002; Prince et al., 1998). Morpholino knockdown of these genes, however, did not result in changes in the Weberian apparatus (our data, not shown). Correspondingly, we found that miR-196 injection led to posteriorizing homeotic transformations or vertebral segment deletion in Weberian vertebrae, which are homologous to vertebrae surrounding the cervical-to-thoracic transition in tetrapods (Burke et al., 1995; Morin-Kensicki et al., 2002). If miR-196 inhibits expression of these *hox* genes, then miR-196-injected animals should show *hox* loss-of-function phenotypes and miR-196 knockdown animals should show *hox* gain-of-function phenotypes, as observed in chick after miR-196 knockdown (McGlinn et al., 2009). In contrast, loss-of-function mutations for mouse orthologs of *hoxb6b*, *hoxc6a*, *hoxb8a* and *hoxb8b* give rise to anteriorizing, not posteriorizing, homeotic transformations at the cervical/thoracic transition (Garcia-Gasca and Spyropoulos, 2000; Rancourt et al., 1995; van den Akker et al., 2001), and *Hoxc8* mutations cause anteriorization of the caudal thoracic vertebrae (van den Akker et al., 2001). How can we understand this discrepancy?

In contrast to most *Hox* genes, *Hoxa5* and *Hoxa6* mutants show a posterior homeotic transformation in the rostral mouse vertebral column (Jeannotte et al., 1993; Kostic and Capecchi, 1994). Mouse *Hoxa5* is expressed with an anterior border in the third cervical vertebra and continuing expression into thoracic vertebrae (Jeannotte et al., 1993); this region is homologous to the zebrafish Weberian vertebrae. Zebrafish has no *hoxa6* gene and has a single *hoxa5* gene (Amores et al., 1998), which is not a predicted miR-196 target and is not expressed in somites (Thisse and Thisse, 2005); the final zebrafish *hox5* paralogy group gene, *hoxc5a*, is also not expressed in somites (Ericson et al., 1993). In addition, genes of the *hoxb* cluster (*hoxb1a* and *hoxb1b*) have newly assumed, or have maintained ancestral, functions equivalent to the same paralogy group but to a different cluster in mouse (*Hoxa1*), a process called 'function shuffling' (McClintock et al., 2002). The *hox1* findings suggest the analogous hypothesis that function shuffling could have occurred between the zebrafish *hoxb5* duplicates and the mouse *Hoxa5* gene. According to this interpretation, the posterior transformations at the cervical/thoracic transition found after *Hoxa5* knockout in mouse, which are similar to the posterior transformations of the homologous region in zebrafish after miR-196 action, are caused by the miR-196-induced inhibition of zebrafish *hoxb5a*, which is expressed in a pattern homologous to that of mouse paralog *Hoxa5* and which we showed to respond to miR-196, at least in the CNS, by changed transcript patterns.

An alternative explanation for miR-196 induced re-patterning is that a Weberian vertebra is missing rather than showing homeotic transformations. Loss of *Hoxa3* and *Hoxd3* function deletes a cervical vertebra in mouse (Horan et al., 1995), and deletion of a zebrafish homolog of a cervical vertebra could mimic the observed posteriorization, causing, for example, the third segment to have the morphology of the fourth vertebra.

miR-196 alters the number of elements in the axial skeleton

Besides pattern changes among Weberian vertebrae, increased and decreased miR-196 levels produced animals with fewer and more ribs than normal, respectively. Morpholino knockdown of *hoxb5a*, *hoxb5b*, *hoxb6b* and *hoxc6a* did not cause changes in rib and vertebral number, while knockdown of *hoxb8a* resulted in one extra rib in 54.5% ($n = 33$) of the animals checked, contradicting the prediction that knockdown of *Hox* gene targets for *mir196* should result in missing ribs and vertebrae. The predicted miR-196 target *hoxa10b* is expressed in somites that give rise to rib-bearing (precaudal) vertebrae with the same anterior border as the non-targets *hoxb10a* and *hoxd10a* (Morin-Kensicki et al., 2002). In mouse, knockdown of *Hoxa10*, a predicted target of miR-196, gives rise to posterior transformations of caudal thoracic vertebrae (Rijli et al., 1995). Overexpression of miR-196 should knockdown *hoxa10b* function, and an accompanying posterior transformation as in mouse could change precaudal, rib-bearing vertebrae into caudal, non-rib-bearing vertebrae, thereby decreasing rib number. Conversely, knockdown of miR-196 could cause overexpression or ectopic expression of *hoxa10b*, which could transform caudal vertebrae to precaudal, rib-bearing vertebrae, thereby increasing the number of vertebrae, as we observed.

A simple one-to-one fate transformation model caudal to the Weberian apparatus does not provide a full explanation of our results because the total number of vertebrae decreased after miR-196 overexpression (up to seven fewer somites than controls) and, reciprocally, increased after miR-196 knockdown (up to four more somites). In normal zebrafish, length variation arises mostly from variation in caudal vertebrae (Morin-Kensicki et al., 2002), whereas length variation in miR-196-manipulated fish involved mostly Weberian and precaudal vertebrae, indicating a difference between the mechanism of miR-196 action and the origin of naturally occurring variation. Somite number variation suggests that miR-196 may interfere with the segmentation clock, the mechanism that dictates the rhythm of somitogenesis from pre-segmental mesoderm (Lewis et al., 2009). Direct players in the

zebrafish segmentation clock (*her1*, *her4*, *her7*, *notch1a*, *notch1b*, *notch5*, *notch6*, *deltaC*, *deltaD*, *Mespa/b*, *ephA4*, *ephrinAl1* and *ephrin-B2*) (Lewis et al., 2009) do not have predicted miR-196 binding sites, suggesting that miR-196 does not act on somite number directly by inhibiting expression of these genes. The expression of miR-196 and several caudal *hox* genes with predicted miR-196 binding sites are co-expressed in the tailbud, and one or more of these are potential targets to explain the somite number effect of miR-196. Our experiments suggest that miR-196 plays a role in somite number, but further work is required to identify the mechanism by which it controls the length of time the segmentation clock continues to run.

Conclusions

These experiments revealed four exquisitely specific viable phenotypes caused by up- or down-regulation of miR-196 levels in zebrafish embryos. Analysis showed that the miR-196-induced failure of fin bud initiation arises from the suppression of retinoic acid signaling in lateral plate mesoderm by fine-tuning expression of the retinoic acid receptor *rarab*, which had previously been shown to be essential for fin bud outgrowth. The inhibition of pharyngeal arch 6 by endogenous or exogenous miR-196 does not arise from the inhibition of any single predicted *hox* target, but from the inhibition of pharyngeal pouch segmentation, about which we currently know little. The posteriorizing effect of miR-196 on vertebrae at a level that corresponds to the cervical-to-thoracic transition are best understood by the differential sorting out of ancestral functions common to *Hoxa* and *Hoxb* genes in zebrafish and tetrapod lineages. Finally, the inhibitory effect of exogenous and endogenous miR-196 on somite number is due to its inhibition of an unknown target, perhaps one or more *hox* genes. These experiments show remarkable parallels between the patterning functions of the protein-coding genes of the *Hox* clusters and a microRNA gene embedded between them.

Methods

Animals

Wild-type fish were ABC/TU hybrids and the *Tg(fli1:EGFP)*^{y1} line (alias *fli-GFP*) (Lawson and Weinstein, 2002) provided animals with labeled cranial crest. The *Tg(RARE-gata2:NTD-eYFP)ld1* line (Perz-Edwards et al., 2001) provided RA signaling reporters. The *cyp26a1*^{rw716} mutant fish was kindly provided by Lei Feng (C. Moens laboratory). Skeleton preparations were as described (Walker and Kimmel, 2007). Experiments involving animals used protocols approved by the University of Oregon IACUC.

Injections

Morpholino oligonucleotide (MO, Gene Tools) sequences were: *mir196a*-MO: AATCCCAACAACATGAAACTACCTAA, *mir196b* mutiple blocking (MB) -MO: ACGTCCAGCCCAACAACTTGAAACTACCTAA. Experiments utilized the GeneTools 'control' morpholino CCTCTTACCTCAGTTACAATTTATA. We injected one-cell stage zebrafish embryos with approximately 3 nL of these two MOs at a final concentration of 1.5 mM *mir196a*MO and 0.5 mM *mir196b*MB-MO. The *rarab*-MO was as reported (Linville et al., 2009). RNA oligonucleotide (Integrated DNA Technology) sequences were: miR-196a: UAGGUAGUUUCAUGUUGUUGGG; miR-196a*: CGACAACAAGAAACUGCCUUGA; miR-196b UAGGUAGUUUCAAGUUGUUGGG; miR-196b*: CAGGAACCUGAAACUGCCUGAA; miR-196bmm (mismatch control): UUCCGUCAAUCAAGUUGUUGGG. Because 3 nL of 12.5 μM stock of miR-196a or miR-196b duplexes yielded identical phenotypes, we used miR-196b duplex for most experiments.

Reporter constructs

From genomic DNA, we amplified a 1349 nt fragment of the 3′UTR of *rarab* (primers: rarab + 314: GTAGACTTTGACCCGGACTGAACA and rarab-1639: AGAAGGCTTTTGGGTGAACTATCC) containing all three predicted miR-196 binding sites and inserted it into pCR4-TOPO (Invitrogen). To fuse *GFP* with the *rarab* 3′ UTR, we used NotI and SpeI to liberate the *rarab* 3′UTR from pCR4-TOPO and used NotI and XhoI to extract *GFP* from pEGFP-N3 (Clontech). To make the *GFP-rarab3′*UTR construct, we ligated fragments into PCRII-TOPO (Invitrogen) between SpeI and XhoI sites. To make the luciferase reporter, ptkLuc+ vector was digested with NgoMIV and KpnI and the fragment was ligated to the *rarab* 3′UTR that was cloned from genomic DNA by the above primers containing NgoMIV and KpnI sites (primers: rarab + 314NgoMIV: gggccggcGTAGACTTTGACCCGGACTGAACA and rarab-1639KpnI: ggggtaccAGAAGGCTTTTGGGTGAACTATCC; small letters represent linkers added for cloning). To make GFP-*rarab3′*UTR mRNA, the construct PCRII-GFP-rarab3′UTR was linearized with SpeI and transcribed in vitro using mMESSAGE mMACHINE T7 kit (Ambion). GFP-*rarab*3′UTR mRNA was purified with an RNA clean-up kit (Zymo Research) and diluted to 15 μL with nuclease-free water to store in −80 °C. For co-injections, we injected first 200 ng/μL of the synthetic *GFP-rarab* 3′UTR mRNA and then *mir196* morpholino mix or 12.5 μM miR-196 duplex or miR-196bmm control.

To make the GFP-*rarab*-mut3′UTR construct, the following primers were used to skip the predicted binding sites for miR-196 in the 3′UTR of *rarab*: rarab + 314NotI gggcggccgcTAGACTTTGACCCGGACTGAACA; rarabUTR-430XhoI ggctcgagGCTCTTGTAGTCGCTGAATC; rarabUTR + 468XhoI ggctcgagCTTCACAGAGATGACAGAACA; rarabUTR-1393sacII ttggccgcggTAAAGTACAGAAGAAGAGGAA; rarabUTR + 1479sacII ttccgcggTGTGACAATCACTTCAAGTAA; and rarabUTR-1639SpeI ggactagtAGAAGGCTTTTGGGTGAACTATCC. PCR products were digested by restriction enzymes identified in the primer names and were sequentially ligated for insertion into GFP downstream of the same vector for GFP-*rarab3′*UTR. mRNA was synthesized and injected and scored as for GFP-*rarab3′*UTR.

Similarly, The *hoxb8a* 3′UTR was cloned into pCR4 vector by the primer pairs: *hoxb8a* + 1081 CCGGCGAAGACTGCGACAA; *hoxb8a*-1731 ACCCCAAGAAAGGAAGACAACAAA and replaced *rarab* 3′UTR in pCRII-GFP for GFP reporter assay. The 3′UTR of *cyp26a1* was cloned using the primer pair: *cyp26a1* + NgoMIV ggcgccggcGGACCCCCGACAATGAAAAC; *cyp26a1*-KpnI: ggcggtacCGAACAGTCTGGGTATGTTAAAT (small letters represent linkers added for the cloning) and replaced *rarab* 3′UTR of ptkLuc-*rarab3′*UTR for the *cyp26a1* 3′UTR reporter assay.

Reporter assay

One cell embryos were injected with 3 μL of a 200 ng/μL solution of GFP-*rarab3′*UTR or GFP-*hoxb8a3′*UTR mRNA and then were co-injected with 1 μL of a solution of 12.5 μM miR-196 duplex or 2 mM *mir196*-MO. Embryos raised at 28.5 °C to 28 hpf were imaged in 3% methylcellulose. To quantify GFP intensity, we used Photoshop, selected fuzziness to 40 and used the "select" and "color range" function to set a threshold, then used the histogram function to calculate the numbers and standard deviation of the green pixels. For the luciferase assay in 293T cells, we used the original ptkLuc+ vector for which luciferase expression is driven by a thymidine kinase promoter with luciferase flanked by either rarab 3′UTR or SV40 polyadenylation signal as a control. For the assay, either 50 ng of ptkLuc+ control plasmid or ptKLuc-*rarab* 3′UTR with 10 ng of CMV-*Renilla* plasmid and 200 ng miR-196 duplex were co-transfected. Cells were harvested at 2-hour intervals from 4 to 12 h after transfection. Firefly and *Renilla* (sea pansy) luciferase activities were both directly quantified within each sample directly after cell lysis (Dual-*Luciferase* Reporter Assay System, Promega) and the firefly luciferase activity was calculated relative to the *Renilla* luciferase control. In addition, the

relative luciferase activity of ptkLuc-*rarab* 3′UTR construct was normalized to the ptkLuc+ control.

For the ptkLuc-*cyp26a13*′UTR assay, 50 ng of *ptkLuc-cyp26a13*′UTR construct or ptkLuc+ control vector together with 10 ng of *Renilla* luciferase construct, 40 ng of miR196 duplex or miR196mm duplex per well were mixed and transfected with 0.3 μL FuGENE HD transfection reagent (http://www.roche.com) into 293T cells in a 96-well plate. Twenty-four hours after transfection, firefly and *Renilla* luciferase activity was assayed by using the Promega Dual-Glo Luciferase Assay System (http://www.promega.com). This experiment was repeated 6 times. Standard deviation was plotted as error bars.

RA treatment

A stock solution of 10^{-3} M all-trans retinoic acid (RA) (Sigma cat# R2625) was prepared in DMSO and stored at −80 °C. Zebrafish embryos were dechorionated in embryo medium and the stock DEAB solution was added to 5 mL embryo medium at a final concentration of 10^{-5} M or 5×10^{-6} M. Twelve hours post-fertilization embryos were treated for 2 h to elevate the level of RA during pectoral fin induction. Treatment was carried out in a dark environment. After treatment, embryos were washed in fresh medium twice and then cultured in fresh medium until fixed. 0.5 μL DMSO was added to the control embryo medium as a negative control.

DEAB treatment

A stock solution of 10^{-2} M 4-Diethylaminobenzaldehyde (DEAB) (Sigma cat# R86256) was prepared in DMSO and stored at −80 °C. Zebrafish embryos were dechorionated in embryo medium before treatment. DEAB at a final concentration of 10 μM was added into fresh embryo medium from 100% epiboly to 24 hpf and then were fixed at various times later. Treatment was carried out in a dark environment. After treatment, embryos were washed twice in embryo medium and cultured in fresh medium until fixed. DMSO with the same concentration was used as a negative control.

Cloning and in situ hybridization

To generate PCR products containing partial *mir196* primary transcript, we used 1 dpf zebrafish whole embryo cDNA reverse transcribed with oligo-dT primer. Cloning of *mir196* primary transcripts used the primers: mir196a1 + 523 ATTAAATGAACGCTAGCGGCTGTATGATG, mir196a1-1014 TTTTGCTAGCGCTTTGTCTTTGTAACCA; mir196a2 + 1349 GCAGACAGGAGAGCGGCAAGAA, mir196a2-1891 AGCAGGCAAGGCAAGATTATGGTA; mir196b + 756 GTATCTCTTTGCCCCGCTGTGG, mir196b-1292 TGGAAAAACGATGGGAAAGTATTG; mir196c + 1016 ATTGCTTTAGATTATGCGCGGGTATTT, mir196c-1339 CAAGCTATGTCAAGGCGTGTCTGTCT; mir196d + 467 TATGCTACCTGGTGCCGTGAAG, mir196d-1325 CCGCTGATAATGGAAGACAACC. Gene sequences were submitted to NCBI GenBank with the following nucleotide sequence accession numbers: dre-mirn196a-1, GU188984; dre-mirn196a-2, GU188985; dre-mirn196b, GU188986; dre-mirn196c, GU188987; and dre-mirn196d, GU188988. Other probes were cloned with primers: beta actin + 184 TGGTTGGCATGGGACAGAAAGA, bactin-556 ATGGCATGGGGAAGAGCGTAAC; tbx5 + 305 TCAACAGGGAATGGAGGGAATCAAA, tbx5-1213 AGAGTAGCTTAGGGGCCGGTAGTAGTGGT; fgf10a + 11 ATGCCCCTCGTCGCCTCTTATTCTG, fgf10a-1458 TTCCCTGGTGCCAATAACTTAAACAA; wnt2b + 344 GGTGGTACATTGGTGCGTTAGGAG, wnt2b-1304 GCCAGTCGGGTTTCTTGTGTAGTT; prdm1 + 2208 GAGGGCATGGTGGAGAAGCAGATA, prdm1-3391 AAAGGCCGAGGTGACGTGAAGAGT; *lbx1b* was from Dr. Haruki Ochi (nt 67 to 810 of NM_001025532) and *fgf24* probe was as described (Fischer et al., 2003). PCR products were cloned into pCR4-TOPO (Invitrogen) vector and *in situ* hybridization was as described (Hale et al., 2006). Antisense LNA (locked nucleic acid) probe for miR-196a with the sequence, 5′Dig/CCCAACAACATGAAACTACCTA/3′Dig, was ordered from Exiqon (http://Exiqon.com) and in situ hybridization was according to the manufacturer.

RT-PCR and qPCR analyses

From each experimental and control group, total RNA was isolated from 50 zebrafish embryos at 27 hpf using the RoboZol RNA extraction reagent for total RNA including microRNA (Amresco Cat: N580-100ML). Two micrograms total RNA from each sample was reverse transcribed into cDNA for qPCR using Mir-X™ miRNA First-Strand Synthesis and SYBR® qRT-PCR (Clontech, cat:PT4445-1). A 1/70th aliquot of each microRNA cDNA reaction was used in a 20 μL qPCR amplification reaction and qPCR assayed in StepOnePlus (Applied Biosystem). Primer sequences were miR-196a TAGGTAGTTTCATGTTGTTGGG and miR-196b TAGGTAGTTTCAAGTTGTTGGG. The relative expressions of miR-196a and miR196b were normalized to the U6 spliceosomal RNA provided in the Mir-X™ miRNA First-Strand Synthesis and SYBR® qRT-PCR kit (Clontech). The comparative C_T experimental method was used to calculate the normalized relative expression level of the target gene from triplicate measurements. Averaged plots for triplicate qPCR reactions for each relative quantitation are shown in Supplemental Fig. 10. Cycling conditions for KAPA SYBR® FAST ABI Prism® 2× qPCR Master Mix (KAPA Biosystems, Cat: KK4603) consisted of 95 °C, 10 min followed by 40 cycles of 95 °C, 60 °C 20 s and then dissociate at 95 °C, 1 min, 55 °C, 30 s and 95 °C, 30 s.

Supplementary materials related to this article can be found online at doi:10.1016/j.ydbio.2011.07.014.

Acknowledgments

We thank Charles Kimmel, Judith Eisen, and Cristian Cañestro for helpful discussions, Haruki Ochi for the gift of a plasmid, Lei Feng for *cyp26a1* mutant fish, Ruth BreMiller for help with histology, Amanda Rapp for animal care, J.T. Neal help for QPCR, Catherine Wilson for help with statistics, and Jesse Buss and Jiin Park for undergraduate research help. The work was supported by DAAD through the Graduate School of Life Sciences, University of Würzburg (XH), the Deutsche Forschungsgemeinschaft (grant GRK 1048 (MS)), Alexander von Humboldt Foundation (JHP), and the National Institutes of Health (grants 5 P01 HD22486, 1 R01 RR020833, and 1 U01 DE020076 (JHP)). Support agencies played no role in study design, in the collection, analysis or interpretation of data, in the writing of the report, or in the decision to submit the paper for publication.

References

Amores, A., Force, A., Yan, Y.L., Joly, L., Amemiya, C., Fritz, A., Ho, R.K., Langeland, J., Prince, V., Wang, Y.L., Westerfield, M., Ekker, M., Postlethwait, J.H., 1998. Zebrafish hox clusters and vertebrate genome evolution. Science 282, 1711–1714.

Amores, A., Suzuki, T., Yan, Y.L., Pomeroy, J., Singer, A., Amemiya, C., Postlethwait, J.H., 2004. Developmental roles of pufferfish Hox clusters and genome evolution in ray-fin fish. Genome Res. 14, 1–10.

Asli, N.S., Kessel, M., 2010. Spatiotemporally restricted regulation of generic motor neuron programs by miR-196-mediated repression of Hoxb8. Dev. Biol. 344, 857–868.

Bagnall, K.M., Higgins, S.J., Sanders, E.J., 1988. The contribution made by a single somite to the vertebral column: experimental evidence in support of resegmentation using the chick–quail chimaera model. Development 103, 69–85.

Bayha, E., Jorgensen, M.C., Serup, P., Grapin-Botton, A., 2009. Retinoic acid signaling organizes endodermal organ specification along the entire antero-posterior axis. PLoS One 4, e5845.

Begemann, G., Schilling, T.F., Rauch, G.J., Geisler, R., Ingham, P.W., 2001. The zebrafish neckless mutation reveals a requirement for raldh2 in mesodermal signals that pattern the hindbrain. Development 128, 3081–3094.

Bird, N.C., Mabee, P.M., 2003. Developmental morphology of the axial skeleton of the zebrafish, *Danio rerio* (Ostariophysi: Cyprinidae). Dev. Dyn. 228, 337–357.

Birkholz, D.A., Olesnicky Killian, E.C., George, K.M., Artinger, K.B., 2009. Prdm1a is necessary for posterior pharyngeal arch development in zebrafish. Dev. Dyn. 238, 2575–2587.

Bruce, A.E., Oates, A.C., Prince, V.E., Ho, R.K., 2001. Additional hox clusters in the zebrafish: divergent expression patterns belie equivalent activities of duplicate hoxB5 genes. Evol. Dev. 3, 127–144.
Burke, A.C., Nelson, C.E., Morgan, B.A., Tabin, C., 1995. Hox genes and the evolution of vertebrate axial morphology. Development 121, 333–346.
Chambers, K.E., McDaniell, R., Raincrow, J.D., Deshmukh, M., Stadler, P.F., Chiu, C.H., 2009. Hox cluster duplication in the basal teleost *Hiodon alosoides* (Osteoglossomorpha). Theory Biosci. 128, 109–120.
Chen, F., Capecchi, M.R., 1997. Targeted mutations in hoxa-9 and hoxb-9 reveal synergistic interactions. Dev. Biol. 181, 186–196.
Chen, C., Zhang, Y., Zhang, L., Weakley, S.M., Yao, Q., 2011. MicroRNA-196: critical roles and clinical applications in development and cancer. J. Cell. Mol. Med. 15, 14–23.
Crump, J.G., Maves, L., Lawson, N.D., Weinstein, B.M., Kimmel, C.B., 2004. An essential role for Fgfs in endodermal pouch formation influences later craniofacial skeletal patterning. Development 131, 5703–5716.
Davis, A.P., Witte, D.P., Hsieh-Li, H.M., Potter, S.S., Capecchi, M.R., 1995. Absence of radius and ulna in mice lacking hoxa-11 and hoxd-11. Nature 375, 791–795.
Di-Poi, N., Koch, U., Radtke, F., Duboule, D., 2010. Additive and global functions of HoxA cluster genes in mesoderm derivatives. Dev. Biol. 341, 488–498.
Duboule, D., Morata, G., 1994. Colinearity and functional hierarchy among genes of the homeotic complexes. Trends Genet. 10, 358–364.
Dupe, V., Ghyselinck, N.B., Wendling, O., Chambon, P., Mark, M., 1999. Key roles of retinoic acid receptors alpha and beta in the patterning of the caudal hindbrain, pharyngeal arches and otocyst in the mouse. Development 126, 5051–5059.
Emoto, Y., Wada, H., Okamoto, H., Kudo, A., Imai, Y., 2005. Retinoic acid-metabolizing enzyme Cyp26a1 is essential for determining territories of hindbrain and spinal cord in zebrafish. Dev. Biol. 278, 415–427.
Ericson, J.U., Krauss, S., Fjose, A., 1993. Genomic sequence and embryonic expression of the zebrafish homeobox gene hox-3.4. Int. J. Dev. Biol. 37, 263–272.
Finnerty, J.R., Pang, K., Burton, P., Paulson, D., Martindale, M.Q., 2004. Origins of bilateral symmetry: Hox and dpp expression in a sea anemone. Science 304, 1335–1337.
Fischer, S., Draper, B.W., Neumann, C.J., 2003. The zebrafish fgf24 mutant identifies an additional level of Fgf signaling involved in vertebrate forelimb initiation. Development 130, 3515–3524.
Fjose, A., Zhao, X.F., 2010. Exploring microRNA functions in zebrafish. N. Biotechnol.
Garcia-Gasca, A., Spyropoulos, D.D., 2000. Differential mammary morphogenesis along the anteroposterior axis in Hoxc6 gene targeted mice. Dev. Dyn. 219, 261–276.
Garrity, D.M., Childs, S., Fishman, M.C., 2002. The heartstrings mutation in zebrafish causes heart/fin Tbx5 deficiency syndrome. Development 129, 4635–4645.
Gehring, W.J., Kloter, U., Suga, H., 2009. Evolution of the Hox gene complex from an evolutionary ground state. Curr. Top. Dev. Biol. 88, 35–61.
Gibert, Y., Gajewski, A., Meyer, A., Begemann, G., 2006. Induction and prepatterning of the zebrafish pectoral fin bud requires axial retinoic acid signaling. Development 133, 2649–2659.
Graham, A., Papalopulu, N., Krumlauf, R., 1989. The murine and *Drosophila* homeobox gene complexes have common features of organization and expression. Cell 57, 367–378.
Grande, T., Young, B., 2005. The ontogeny and homology of the Weberian apparatus in the zebrafish *Danio rerio* (Ostariophysi: Cypriniformes). Zool. J. Linn. Soc. 104, 241–254.
Grandel, H., Lun, K., Rauch, G.J., Rhinn, M., Piotrowski, T., Houart, C., Sordino, P., Kuchler, A.M., Schulte-Merker, S., Geisler, R., Holder, N., Wilson, S.W., Brand, M., 2002. Retinoic acid signalling in the zebrafish embryo is necessary during pre-segmentation stages to pattern the anterior–posterior axis of the CNS and to induce a pectoral fin bud. Development 129, 2851–2865.
Griffiths-Jones, S., Saini, H.K., van Dongen, S., Enright, A.J., 2008. miRBase: tools for microRNA genomics. Nucleic Acids Res. 36, D154–D158.
Hale, L.A., Tallafuss, A., Yan, Y.L., Dudley, L., Eisen, J.S., Postlethwait, J.H., 2006. Characterization of the retinoic acid receptor genes raraa, rarab and rarg during zebrafish development. Gene Expr. Patterns 6, 546–555.
He, L., Hannon, G.J., 2004. MicroRNAs: small RNAs with a big role in gene regulation. Nat. Rev. Genet. 5, 522–531.
He, X., Eberhart, J.K., Postlethwait, J.H., 2009. MicroRNAs and micromanaging the skeleton in disease, development, and evolution. J. Cell. Mol. Med. 13, 606–618.
Hoffman, L., Miles, J., Avaron, F., Laforest, L., Akimenko, M.A., 2002. Exogenous retinoic acid induces a stage-specific, transient and progressive extension of Sonic hedgehog expression across the pectoral fin bud of zebrafish. Int. J. Dev. Biol. 46, 949–956.
Horan, G.S., Kovacs, E.N., Behringer, R.R., Featherstone, M.S., 1995. Mutations in paralogous Hox genes result in overlapping homeotic transformations of the axial skeleton: evidence for unique and redundant function. Dev. Biol. 169, 359–372.
Hornstein, E., Mansfield, J.H., Yekta, S., Hu, J.K., Harfe, B.D., McManus, M.T., Baskerville, S., Bartel, D.P., Tabin, C.J., 2005. The microRNA miR-196 acts upstream of Hoxb8 and Shh in limb development. Nature 438, 671–674.
Hou, W., Tian, Q., Zheng, J., Bonkovsky, H.L., 2010. Zinc mesoporphyrin induces rapid proteasomal degradation of hepatitis C nonstructural 5A protein in human hepatoma cells. Gastroenterology 138, 1909–1919.
Huang, R., Zhi, Q., Patel, K., Wilting, J., Christ, B., 2000. Contribution of single somites to the skeleton and muscles of the occipital and cervical regions in avian embryos. Anat. Embryol. (Berl) 202, 375–383.
Jarinova, O., Hatch, G., Poitras, L., Prudhomme, C., Grzyb, M., Aubin, J., Berube-Simard, F.A., Jeannotte, L., Ekker, M., 2008. Functional resolution of duplicated hoxb5 genes in teleosts. Development 135, 3543–3553.
Jeannotte, L., Lemieux, M., Charron, J., Poirier, F., Robertson, E.J., 1993. Specification of axial identity in the mouse: role of the Hoxa-5 (Hox1.3) gene. Genes Dev. 7, 2085–2096.
Kawasaki, H., Taira, K., 2004. MicroRNA-196 inhibits HOXB8 expression in myeloid differentiation of HL60 cells. Nucleic Acids Symp. Ser. (Oxf) 211–212.
Kopinke, D., Sasine, J., Swift, J., Stephens, W.Z., Piotrowski, T., 2006. Retinoic acid is required for endodermal pouch morphogenesis and not for pharyngeal endoderm specification. Dev. Dyn. 235, 2695–2709.
Kostic, D., Capecchi, M.R., 1994. Targeted disruptions of the murine Hoxa-4 and Hoxa-6 genes result in homeotic transformations of components of the vertebral column. Mech. Dev. 46, 231–247.
Koudijs, M.J., den Broeder, M.J., Groot, E., van Eeden, F.J., 2008. Genetic analysis of the two zebrafish patched homologues identifies novel roles for the hedgehog signaling pathway. BMC Dev. Biol. 8, 15.
Krumlauf, R., 1994. Hox genes in vertebrate development. Cell 78, 191–201.
Lawson, N.D., Weinstein, B.M., 2002. In vivo imaging of embryonic vascular development using transgenic zebrafish. Dev. Biol. 248, 307–318.
Lewis, J., Hanisch, A., Holder, M., 2009. Notch signaling, the segmentation clock, and the patterning of vertebrate somites. J. Biol. 8, 44.
Li, Y., Zhang, M., Chen, H., Dong, Z., Ganapathy, V., Thangaraju, M., Huang, S., 2010. Ratio of miR-196s to HOXC8 messenger RNA correlates with breast cancer cell migration and metastasis. Cancer Res. 70, 7894–7904.
Linville, A., Radtke, K., Waxman, J.S., Yelon, D., Schilling, T.F., 2009. Combinatorial roles for zebrafish retinoic acid receptors in the hindbrain, limbs and pharyngeal arches. Dev. Biol. 325, 60–70.
Lund, A.H., 2009. miR-10 in development and cancer. Cell Death Differ.
Ma, L., Teruya-Feldstein, J., Weinberg, R.A., 2007. Tumour invasion and metastasis initiated by microRNA-10b in breast cancer. Nature 449, 682–688.
McClintock, J.M., Kheirbek, M.A., Prince, V.E., 2002. Knockdown of duplicated zebrafish hoxb1 genes reveals distinct roles in hindbrain patterning and a novel mechanism of duplicate gene retention. Development 129, 2339–2354.
McGlinn, E., Yekta, S., Mansfield, J.H., Soutschek, J., Bartel, D.P., Tabin, C.J., 2009. In ovo application of antagomiRs indicates a role for miR-196 in patterning the chick axial skeleton through Hox gene regulation. Proc. Natl. Acad. Sci. U.S.A. 106, 18610–18615.
McIntyre, D.C., Rakshit, S., Yallowitz, A.R., Loken, L., Jeannotte, L., Capecchi, M.R., Wellik, D.M., 2007. Hox patterning of the vertebrate rib cage. Development 134, 2981–2989.
Mercader, N., 2007. Early steps of paired fin development in zebrafish compared with tetrapod limb development. Dev. Growth Differ. 49, 421–437.
Mercader, N., Fischer, S., Neumann, C.J., 2006. Prdm1 acts downstream of a sequential RA, Wnt and Fgf signaling cascade during zebrafish forelimb induction. Development 133, 2805–2815.
Minoux, M., Antonarakis, G.S., Kmita, M., Duboule, D., Rijli, F.M., 2009. Rostral and caudal pharyngeal arches share a common neural crest ground pattern. Development 136, 637–645.
Morin-Kensicki, E.M., Melancon, E., Eisen, J.S., 2002. Segmental relationship between somites and vertebral column in zebrafish. Development 129, 3851–3860.
Niederreither, K., Subbarayan, V., Dolle, P., Chambon, P., 1999. Embryonic retinoic acid synthesis is essential for early mouse post-implantation development. Nat. Genet. 21, 444–448.
Nolte, C., Amores, A., Nagy Kovacs, E., Postlethwait, J., Featherstone, M., 2003. The role of a retinoic acid response element in establishing the anterior neural expression border of Hoxd4 transgenes. Mech. Dev. 120, 325–335.
Oliver, G., De Robertis, E.M., Wolpert, L., Tickle, C., 1990. Expression of a homeobox gene in the chick wing bud following application of retinoic acid and grafts of polarizing region tissue. EMBO J. 9, 3093–3099.
Perz-Edwards, A., Hardison, N.L., Linney, E., 2001. Retinoic acid-mediated gene expression in transgenic reporter zebrafish. Dev. Biol. 229, 89–101.
Postlethwait, J.H., Schneiderman, H.A., 1969. A clonal analysis of determination in Antennapedia a homeotic mutant of *Drosophila melanogaster*. Proc. Natl. Acad. Sci. U.S.A. 64, 176–183.
Postlethwait, J.H., Yan, Y.L., Gates, M.A., Horne, S., Amores, A., Brownlie, A., Donovan, A., Egan, E.S., Force, A., Gong, Z., Goutel, C., Fritz, A., Kelsh, R., Knapik, E., Liao, E., Paw, B., Ransom, D., Singer, A., Thomson, M., Abduljabbar, T.S., Yelick, P., Beier, D., Joly, J.S., Larhammar, D., Rosa, F., Westerfield, M., Zon, L.I., Johnson, S.L., Talbot, W.S., 1998. Vertebrate genome evolution and the zebrafish gene map. Nat. Genet. 18, 345–349.
Prince, V.E., Joly, L., Ekker, M., Ho, R.K., 1998. Zebrafish hox genes: genomic organization and modified colinear expression patterns in the trunk. Development 125, 407–420.
Rancourt, D.E., Tsuzuki, T., Capecchi, M.R., 1995. Genetic interaction between hoxb-5 and hoxb-6 is revealed by nonallelic noncomplementation. Genes Dev. 9, 108–122.
Rijli, F.M., Matyas, R., Pellegrini, M., Dierich, A., Gruss, P., Dolle, P., Chambon, P., 1995. Cryptorchidism and homeotic transformations of spinal nerves and vertebrae in Hoxa-10 mutant mice. Proc. Natl. Acad. Sci. U.S.A. 92, 8185–8189.
Rusinov, V., Baev, V., Minkov, I.N., Tabler, M., 2005. MicroInspector: a web tool for detection of miRNA binding sites in an RNA sequence. Nucleic Acids Res. 33, W696–W700.
Sakaguchi, S., Nakatani, Y., Takamatsu, N., Hori, H., Kawakami, A., Inohaya, K., Kudo, A., 2006. Medaka unextended-fin mutants suggest a role for Hoxb8a in cell migration and osteoblast differentiation during appendage formation. Dev. Biol. 293, 426–438.
Sehm, T., Sachse, C., Frenzel, C., Echeverri, K., 2009. miR-196 is an essential early-stage regulator of tail regeneration, upstream of key spinal cord patterning events. Dev. Biol. 334, 468–480.
Sparrow, D.B., Chapman, G., Turnpenny, P.D., Dunwoodie, S.L., 2007. Disruption of the somitic molecular clock causes abnormal vertebral segmentation. Birth Defects Res C Embryo Today. 81, 93–110.
Taylor, J.S., Braasch, I., Frickey, T., Meyer, A., Van de Peer, Y., 2003. Genome duplication, a trait shared by 22 000 species of ray-finned fish. Genome Res. 13, 382–390.
Thatcher, E.J., Paydar, I., Anderson, K.K., Patton, J.G., 2008. Regulation of zebrafish fin regeneration by microRNAs. Proc. Natl. Acad. Sci. U.S.A. 105, 18384–18389.
Thisse, C., Thisse, B., 2005. High Throughput Expression Analysis of ZF-Models Consortium Clones. ZFIN Direct Data Submission. http://zfin.org.

Trevarrow, B., Marks, D.L., Kimmel, C.B., 1990. Organization of hindbrain segments in the zebrafish embryo. Neuron 4, 669–679.
van den Akker, E., Fromental-Ramain, C., de Graaff, W., Le Mouellic, H., Brulet, P., Chambon, P., Deschamps, J., 2001. Axial skeletal patterning in mice lacking all paralogous group 8 Hox genes. Development 128, 1911–1921.
Vella, M.C., Choi, E.Y., Lin, S.Y., Reinert, K., Slack, F.J., 2004. The *C. elegans* microRNA let-7 binds to imperfect let-7 complementary sites from the lin-41 3′UTR. Genes Dev 18, 132–137.
Wakahara, T., Kusu, N., Yamauchi, H., Kimura, I., Konishi, M., Miyake, A., Itoh, N., 2007. Fibin, a novel secreted lateral plate mesoderm signal, is essential for pectoral fin bud initiation in zebrafish. Dev. Biol. 303, 527–535.
Walker, M.B., Kimmel, C.B., 2007. A two-color acid-free cartilage and bone stain for zebrafish larvae. Biotech. Histochem. 82, 23–28.
Waxman, J.S., Keegan, B.R., Roberts, R.W., Poss, K.D., Yelon, D., 2008. Hoxb5b acts downstream of retinoic acid signaling in the forelimb field to restrict heart field potential in zebrafish. Dev Cell. 15, 923–934.
Wellik, D.M., 2009. Hox genes and vertebrate axial pattern. Curr. Top. Dev. Biol. 88, 257–278.
Wendling, O., Ghyselinck, N.B., Chambon, P., Mark, M., 2001. Roles of retinoic acid receptors in early embryonic morphogenesis and hindbrain patterning. Development 128, 2031–2038.
Wienholds, E., Kloosterman, W.P., Miska, E., Alvarez-Saavedra, E., Berezikov, E., de Bruijn, E., Horvitz, H.R., Kauppinen, S., Plasterk, R.H., 2005. MicroRNA expression in zebrafish embryonic development. Science 309, 310–311.
Woltering, J.M., Durston, A.J., 2006. The zebrafish hoxDb cluster has been reduced to a single microRNA. Nat. Genet. 38, 601–602.
Woltering, J.M., Durston, A.J., 2008. MiR-10 represses HoxB1a and HoxB3a in zebrafish. PLoS ONE 3, e1396.
Wotton, K.R., Weierud, F.K., Dietrich, S., Lewis, K.E., 2008. Comparative genomics of Lbx loci reveals conservation of identical Lbx ohnologs in bony vertebrates. BMC Evol. Biol. 8, 171.
Yekta, S., Shih, I.H., Bartel, D.P., 2004. MicroRNA-directed cleavage of HOXB8 mRNA. Science 304, 594–596.
Yekta, S., Tabin, C.J., Bartel, D.P., 2008. MicroRNAs in the Hox network: an apparent link to posterior prevalence. Nat. Rev. Genet. 9, 789–796.